Agricultural and Forest Meteorology 318 (2022) 108915

Contents lists available at ScienceDirect

Agricultural and Forest Meteorology

journal homepage: www.elsevier.com/locate/agrformet

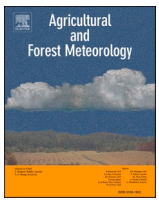

Future shifts in the phenology of table grapes on Crete under a warming climate

Manolis G. Grillakis [a,b,*], Georgios Doupis [c], Evangelos Kapetanakis [b], Eleni Goumenaki [b]

[a] Lab of Geophysical-Remote Sensing and Archaeoenvironment, Institute for Mediterranean Studies, Foundation for Research and Technology Hellas, Rethymno 74100, Greece
[b] School of Agricultural Sciences, Hellenic Mediterranean University, Heraklion, Greece
[c] Institute of Olive Tree, Subtropical Crops and Viticulture, Hellenic Agricultural Organization DEMETER, Chania, Greece

ARTICLE INFO

Keywords:
Climate change
Vitis vinifera
Thompson seedless
Sultana
Phenological model
Growing degree-days

ABSTRACT

Climate change is expected to pose major challenges to viticulture. The projected increase in temperature in the Mediterranean region due to climate change is likely to influence the timing of grapevine phenological stages. This study developed and validated a phenological model, from budbreak to maturation phenological stages, based on the growing degree days for the Sultana grapevine cultivar on Crete Island, Greece, and used the model to assess potential changes in future phenology timing employing different climate change scenarios. A dataset of unpublished phenological observations from 20 locations spanning four decades was used to validate the phenological model. The root mean squared difference (RMSD) of the calibration-validation procedure was estimated between 5.4 and 11.5 days, depending on the phenological stage. The model outperformed for the flowering and maturity stages. The highest RMSD was found for the shoot development stages. Projections determined an earlier occurrence of the different phenological stages. Near future climate (2020–2060) projections indicate budbreak advancement by 7 to 8 days and maturity by 4 to 5 days on average. For the far future (2060–2100), the respective changes are 11 to 18 and 7 to 9 days earlier. Discussion on the underlying uncertainty sources is provided.

1. Introduction

Due to its impacts on crop quality and yield, climate is a key factor determining the economic sustainability of agricultural production. Climate is a determinant factor in agricultural production systems defining crop suitability, influencing yield and quality, and consequently ruling economic sustainability. Many climate scenarios predict changes to future temperature and precipitation regimes, including more frequent extreme heat and drought episodes, that are likely to strongly affect many agricultural regions (Rosenzweig et al., 2014). The Mediterranean region is considered a climate change hot spot (Giorgi and Lionello, 2008; Thiébault et al., 2016; Tramblay et al., 2020).

Studies have consistently reported that climate change is expected to increase summer temperatures, especially in the southern parts of Europe, by the end of the 21st century. Projections for the south-eastern Mediterranean region indicate that the temperature is likely to increase by between 1.7 °C and 2.5 °C for the representative concentration pathway (RCP) 4.5 and between 3.5 °C and 5.0 °C for RCP8.5 (Zittis et al., 2019). These changes are expected to affect plant phenology (De Ollas et al., 2019), the duration of the growing season and the quiescence period and potentially reduce crop productivity and degrade quality (Gordo and Sanz, 2010).

Viticulture has a very high economic importance for Mediterranean Europe as a source of a variety of products, including wines and spirits, table grapes, raisins and fresh grape juice. The annual developmental cycle of the grapevine consists of a dormant period and a growth period, which is further divided into four phases reflecting the concurrent development of vegetative and reproductive organs of the plant. The first phase extends from endodormancy, followed by ecodormancy, to budburst. The second phase encompasses the period from budburst to flowering when vegetative organs and floral structures are developing. The third phase lasts from flowering to veraison. During this phase, the plant actively accumulates biomass, and the berries grow in size through cell division. In the last phase, from veraison to harvest, vegetative

* Corresponding author at: Lab of Geophysical-Remote Sensing and Archaeoenvironment, Institute for Mediterranean Studies, Foundation for Research and Technology Hellas, Rethymno 74100, Greece.
E-mail address: grillakis@hydrogaia.gr (M.G. Grillakis).

https://doi.org/10.1016/j.agrformet.2022.108915
Received 24 December 2020; Received in revised form 13 March 2022; Accepted 18 March 2022
Available online 26 March 2022

growth slows, and berries accumulate sugars and ripen. Three scales are typically used to describe the succession of vine growth stages. These are the Baggiolini scale (Baggiolini, 1952; Baillod and Baggiolini, 1993), the Eichhorn and Lorenz phenological (ELP) scale (Eichhorn and Lorenz, 1977) and the **B**iologische **B**undesanstalt, Bundessortenamt und **CH**emische Industrie (BBCH) scale (Lorenz et al., 1994). Each scale was designed to serve specific needs, exhibiting different advantages and shortcomings. The Baggiolini scale, for example, is a categorical scale that is easy to interpret but difficult to simulate by a statistical model. The BBCH system is used as a code to describe the phenological stages of various monocot and dicot plants. However, it tends to fragment the development stages rather than provide a continuous flow of phenology stages (Coombe, 1995). The Eichhorn and Lorenz Phenological (ELP) scale, which can be accurately reproduced by mathematical models (Fernández-González et al., 2013; Verdugo-Vásquez et al., 2017), is designed specifically for grapevine phenology and covers all growth stages from winter bud (ELP = 1) to the end of leaf fall (ELP = 47).

Climatic factors play a vital role in the terroir of a grapevine growing region, as they strongly control canopy microclimate, plant growth and physiology, yield, and grape berry attributes (Doupis et al., 2020; Jones et al., 2005; Koufos et al., 2018). Air temperature is among the most influential meteorological qualities controlling grapevine development (Santibáñez et al., 2014). Increasing temperatures have been shown to seriously affect vine phenology (Scranton and Amarasekare, 2017). Urhausen et al. (2011) correlated a trend towards earlier budburst and flowering in Upper Moselle, Germany, with increasing temperatures in the region. Along the same lines, Tomasi et al. (2011) studied vine phenological data collected between 1964 and 2009 in the Veneto Region of Italy and found that the onset of events, such as bloom, veraison, and harvest, occurred between 13 and 19 days earlier at the end of the study period. A more extensive study by García de Cortázar-Atauri et al. (2017), who recorded the phenological patterns of 43 vine cultivars in France, found that the timing of budbreak, flowering and veraison trended earlier during the last 30 years. Ruml et al. (2016) analyzed the onset dates of four major phenological stages, along with the corresponding growth intervals between them, for 20 wine grape cultivars in Serbia. Their results indicated that all phenological stages, except budburst, were advanced by −0.4, −0.7 and −0.6 days/year for flowering, veraison and harvest, respectively.

Additionally, numerous studies suggest that predicted changes in climate variables will further influence the viticulture sector worldwide. Ramos and Jones (2018) analyzed the potential changes in the phenology of the Cabernet Sauvignon cultivar under RCP4.5 and RCP8.5 in different future periods. They quantified the timing of vine phenology stages under warming conditions using growing degree days (GDDs) and found that veraison is expected to advance by 24 and 36 days by 2070 for RCP4.5 and RCP8.5, respectively. Teslić et al. (2019) reported that the major wine-producing region of Emilia-Romagna may become too hot for grape production by the end of the century according to RCP8.5. Similarly, Omazić et al. (2020) studied different bioclimatic indices using regional climate models (RCMs) for Croatia and found that further temperature increases and a lack of precipitation events in the area are likely to result in earlier harvests. They also estimated that some of the existing zones and areas where grapevines are grown under favorable climatic conditions will not be suitable for this crop in the future.

Throughout the growing season, grapevines undergo a great number of changes in terms of morphology and physiology. While some grapevine varieties seem to have a fairly similar phenological pattern, they differ in specific morphological and physiological features, resulting in a variety of ripening dates and consequently in early-, mid- and late-season cultivars (Ramos and Jones, 2018; Tomasi et al., 2011). Differences in the timing of flowering and veraison have been extensively studied across a wide range of vine cultivars (Parker et al., 2013). The main factor controlling the timing of vine phenology during the growing season is the temperature regime (Fernández-González et al., 2013; Fraga et al., 2016a; Malheiro et al., 2013). Usually, the impact of temperature on phenology is considered in the form of thermal accumulation above a base temperature (i.e., heat requirements) between phenological intervals, often expressed as GDDs (Parker et al., 2011; Santibáñez et al., 2014; Verdugo-Vásquez et al., 2017). Thermal accumulation has proven to be invaluable for viticultural research (Duchene and Schneider, 2005; Koufos et al., 2014); hence, the concept of GDD has been widely used in the literature. Various forms of thermal accumulation have been used in relevant research, from simple Celsius degree summation to other more sophisticated forms that consider heat stress plants may exhibit beyond certain thresholds. Molitor et al. (2014) assessed the effectiveness of GDD models with variable complexity to describe vine phenology. They found that the more complex GDD models that apply thresholds for plant development stabilization and deceleration significantly improved the accuracy of the model. They resulted in a phenological model with a root mean squared error (RMSE) between 1.8 and 4.7 days. To establish a predictive model of phenological stages based on heat accumulation, Verdugo-Vásquez et al. (2017) found a strong correlation between the ELP scale and GDDs for various table grape cultivars. Their model gained RMSE between 4.4 and 19.4 days. A similar model was used by Santibáñez et al. (2014) in Chile. The approach of Verdugo-Vásquez et al. (2017) and Santibáñez et al. (2014) is also mentioned in the literature as the Mitscherlich monomolecular equation model or Mitscherlich growth. It assumes that the phenological succession is asymptotic to a maximum. It was considered that the end phases of the annual cycle show a deceleration of the rate of development, and this is well expressed by the Mitscherlich equation.

Vine phenological models based on the thermal accumulation, are usually calibrated using site specific phenological observations. Their main limitations are related to the fact that they are simplistic since they consider only thermal forcing, disregarding other climatic and biophysical factors of lesser importance (e.g. water availability or cultivation practices). Further uncertainties in their estimations arise from the thermal forcing estimation and from the quality of the phenological observations used for calibration.

Climate change in relation to viticulture in Greece has been the subject of relatively few studies. Koufos et al. (2014) studied the harvest dates for eight indigenous wine-producing varieties across Greece and related them to climate data using regression modeling. They found a significant correlation between the recent trend of increasing temperature and the earlier onset of grape maturity. Furthermore, they estimate that small island viticulture would be more vulnerable to anticipated changes in temperatures compared to mainland regions. In another study, Lazoglou et al. (2018) assessed the impact of climate change on Greek territories by applying the Geoviticulture Multicriteria Climatic Classification system (Tonietto and Carbonneau, 2004) on the projections of a single regional climate model (RCM). Their findings suggest that increasing temperatures and drought will potentially affect all vine cultivation in Greece. Vineyards at higher altitudes will be positively affected, whereas in islands and coastal regions, there will be a negative impact.

This study employed a phenological model to assess the impact of climate change on *Vitis vinifera* L., the “Sultana” cultivar. Covering an area of more than 270.000 ha, Sultana is the world’s most broadly used variety for table grapes and raisins and to a lesser extent for wines and spirits. It is mainly grown in the East Mediterranean, the Middle East and Central Asia (Greece, Turkey, Iran, Iraq, Afghanistan) and in other continents. Synonyms for this variety in different countries are Soultanina, Kishmish, Soultanine, Thompson seedless, VIVC 12,051 (OIV, 2017). The primary Sultana growing areas in Greece are Crete, Corinthia and Kavala.

The study analyses observational vine phenology datasets that have never been used before in relevant projects. A phenological model was used for the first time to assess changes in growing stage timing under two scenarios of climate change, employing a multimodel RCM ensemble approach never used before in the eastern Mediterranean region. The results constitute a significant addition to the existing

Table 1
Parameter ranges implemented for genetic algorithm optimization.

Parameter	Parameters' range
Eq. (1), parameter Ph_{final}	38–42
Eq. (1), parameter k	0.0010–0.0035
Eq. (1), parameter p	1–5
Eq. (2), parameter a	1–12
Eq. (2), parameter b	15–25
Eq. (2), parameter c	20–30
DoY	1–20

knowledge on the potential climate change impact on sultana-growing regions with similar climate features. This work provides useful insights that can aid adaptation strategies and agricultural system planning to support crop productivity optimization in view of adverse environmental changes. The specific objectives of this work are (a) to calibrate and validate a model for the simulation of phenophase succession in Sultana vines and (b) to use the model to quantify the changes in phenophase timing under two climate change pathway projections and two future periods.

2. Materials and methods

The approaches described by Santibáñez et al. (2014) and Verdugo-Vásquez et al. (2017) were employed to simulate the effects of climate change on the phenological sequence of the grapevine cv. Sultana. These studies suggested a simple phenological model for table grape cultivars based on growing degree days (GDDs). The Santibáñez et al. (2014) formula is shown in Eq. (1).

$$Ph_{stage} = Ph_{final}\left(1 - e^{-kGDD}\right)^{p} \tag{1}$$

where Ph_{stage} is the phenological stage on the ELP scale at any time during the life cycle, Ph_{final} represents the last modeled phenological stage according to the Mitscherlich equation model, k is the shape parameter, which is species dependent, p is the precocity number and GDD is the growing degree days. This formula has been used for various table grape cultivars, including Perlette, Red Globe and Thompson Seedless by Santibáñez et al. (2014) and Thompson, Crimson and Superior Seedless, and Red Globe cultivars by Verdugo-Vásquez et al. (2017). Here, the parameters k and p were considered calibration parameters. Furthermore, as in Santibáñez et al. (2014), Ph_{final} was considered for optimization in the range of the existing literature values (Santibáñez et al., 2014; Verdugo-Vásquez et al., 2017), i.e., 38 to 42.

In Crete, heatwaves during the summer often last long, and their adverse effects are intensified by hot south winds from Africa (Chartzoulakis, 2001), with an observed recent increasing trend (Kuglitsch et al., 2010). In light of these findings, the three-threshold temperature GDD definition of Molitor et al. (2014) was employed, as this approach takes into consideration that the forcing effect of temperature is limited at temperatures higher than the optimal temperature, affecting maturation by causing adverse effects on the photosynthate translocation process (Mori et al., 2007). According to the three-parameter GDD approach, degree days are estimated according to three optimized temperature threshold values, namely, base, upper and heat threshold temperatures. Between the base and the upper temperature values, the forcing effect of temperature is linear, while when temperature crosses the upper threshold, the degree day gain remains stable, and when the temperature surpasses the heat threshold (see below), the degree day accumulation decays linearly. When the temperature exceeds a critical threshold, plant development stops completely, i.e., degree day sum is zeroed. The Molitor et al. (2014) formula for this estimation is shown in Eq. (2):

$$DD\ [^{o}C] = \begin{cases} 0 \ if\ t < a \\ (t-a)\ if\ a < t < b \\ (b-a)\ if\ t > b \\ ((b-a)-(t-c))\ if\ c < t < \ c+(b-a) \\ 0 \ if\ t > c+(b-a) \end{cases} \tag{2}$$

where t is the mean daily temperature, a is the lower threshold temperature, b is the upper threshold temperature and c is the heat threshold temperature. The lower threshold has been defined in the literature as between 0 °C (Parker et al., 2013, 2011) and 10 °C (Santibáñez et al., 2014; Verdugo-Vásquez et al., 2017). Molitor et al. (2014) developed a model to simulate all 26 phenological stages of *the* Müller-Thurgau vine cultivar. They optimized the three-parameter GDD model estimation by testing threshold temperatures between 3 °C and 7 °C for a, 15 °C and 21 °C for b, 21 °C and 24 °C for c, concluding that the best threshold triplet is 5, 20 and 22 °C. These values are entirely experiment-specific but worth mentioning for rough comparison purposes, since in this study, these values were calibrated.

A final parameter to be considered in the GDD estimation is the day of the year (DoY) beyond which the GDDs should be estimated. Garcia de Cortazar Atauri (2006) studied a model to simulate flowering and veraison, starting the GDD count on the 1st of April, while for a similar application, Parker et al. (2011, 2013) used the 1st of March.

The above seven analyzed parameters, shown in Eqs. (1) and (2), were considered for optimization using the genetic algorithm technique. Genetic algorithm optimization is a stochastic, population-based algorithm that searches randomly by mutation and crossover among population members (Breitfeld and Shanno, 1995; Conn et al., 1991; Goldberg, 1989). The optimization was performed using MATLAB®. For the optimization, the parameter space took into consideration the literature values as they were discussed earlier but more relaxed to facilitate potential optimal values outside the existing literature. As an exception, the DoY parameter was considered outside the literature bounds, i.e., between the 1st and 20th of January to precede all cases of phenological observations, as well as potential budbreak dates under climate change. Table 1 shows the parameter range.

Regarding the maturity stage, the ELP considers that scale 38 equals "Berries harvest-ripe (22°Brix)" (Verdugo-Vásquez et al., 2017). Nevertheless, the Sultana cultivar for table grapes is considered harvest-ripe at 16 Brix or more (UNECE, 2017). Therefore, in this work, maturity was considered at ELP >= 37. Calibration of the parameters in (Table 1) was based on the observed phenological data described below. Half of the phenological data were reserved to validate the calibration procedure. The objective function used for the optimization was the root mean squared difference (RMSD) between the simulated and observed days of the year where each ELP stage occurred. The RMSD is shown in Eq. (3):

$$RMSD = \sqrt{\frac{\sum_{1}^{n}\left(DoY_{ELP}^{OBS} - DoY_{ELP}^{SIM}\right)^{2}}{n}} \tag{3}$$

where DoY_{ELP}^{OBS} is the day of the year that each of the n ELP stages was observed, and DoY_{ELP}^{SIM} is the day of the year when the respective ELP stage was simulated. The calibration was based on the minimization of the RMSD. The optimization was performed using the Nelder–Mead optimization algorithm (Lagarias et al., 1998) without constraints.

3. Case study

3.1. The study area

The study was conducted in the vine-growing area on the island of Crete, Greece, the fifth largest island in the Mediterranean. The island covers 8336 Km^2. It is located at the southern limits of the Aegean Sea, at

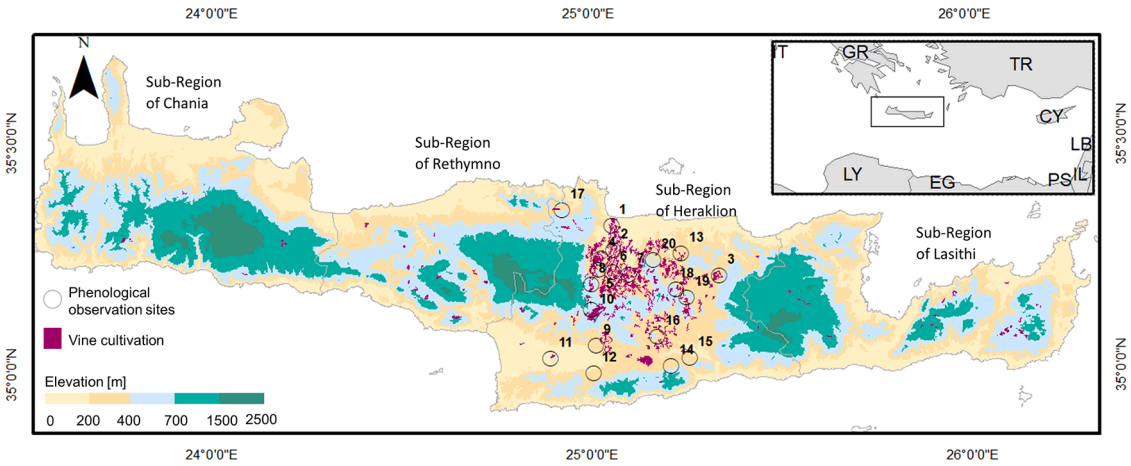

Fig. 1. Phenological observation sites. In purple are the Corine Land Cover 2018 areas occupied by vineyards. Circles indicate the observation sites detailed in Appendix A, Table A1.

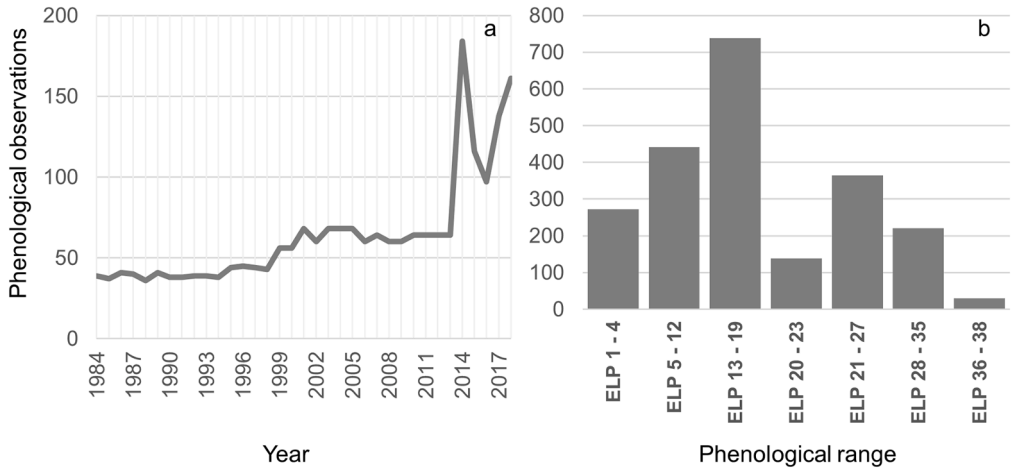

Fig. 2. Phenological observations between 1984 and 2018, (a) number of observations per year, and (b), distribution of observations on the Eichhorn and Lorenz scale, based on the discretization to major growth stages according to (Coombe, 1995).

a distance of approximately 160 km from mainland Greece. The climate on the island is Mediterranean – semiarid, featuring long and dry summers and wet and fairly cold winters. In the Koppen climate classification (Kottek et al., 2006), a considerable part of Crete is categorized as having a Csa (hot-summer Mediterranean) climate. However, a few mountainous regions are categorized as having a Csb (warm-summer Mediterranean climate). These two climate categories are often collectively referred to as "Mediterranean climate", with warm dry summers and cold (but above 0 °C) and wet winters. The elevation of the island varies considerably, between 0 and 2500 m above sea level (Fig. 1). The agricultural sector contributes ca. 8% to the island economy (EC, 2020). The average rainfall on the island is 878 mm/year, exhibiting a decreasing gradient from west to east. It ranges between 440 mm/year on the eastern part of the island and more than 2000 mm/year in the western mountainous regions (Grillakis et al., 2020). In the central parts of the island, where the majority of viticulture is located, the annual precipitation ranges from 500 mm/year in the coastal areas to more than 700 mm/year further inland.

According to the 2018 Corine Land Cover (CLC - Version 20), vineyards on Crete occupy 18,029 ha. Fig. 1 shows the spatial distribution of vine cultivation on the island. The vast majority of the vineyards are located in the central parts of the island in the Sub-Region of Heraklion (for exact positioning, see Table A1 of Appendix A). Vineyards are mainly located at elevations between the coastal areas and 600 m a.s.l.

3.2. Available phenological data

Phenological observations between 1984 and 2018 were obtained from the records of the Regional Center for Plant Protection and Phytosanitary Control of Heraklion (a civil service of the Greek Ministry of Rural Development and Food). This dataset is comprised of more than 2200 phenological observations, from the end of winter to full grape maturity, at 20 sites of Sultana vineyards across the Sub-Region of Heraklion (Fig. 1). Some locations were consistently monitored by the agency during this whole period, while others were monitored for only a few growing seasons. Details about the locations and the number of observations in each of them are shown in Appendix A - Table A1. The phenological observations were recorded using the Baggiolini Phenological scale (Baggiolini, 1952). For the purposes of this study, the Baggiolini scale was converted into the Eichhorn and Lorenz phenological scale using the conversion of Coombe (1995). Fig. 2 shows the varied intensity of observations recorded from 1984 to 2018. The increasing trend of the Sultana observations is because this cultivar replaced others due to of its high profitability as a table grape in the international market (Fig. 2a). Regarding the distribution of the observations during the growing season, the majority of the observations were recorded between the ELP5 stage (just after budburst) and fruit set, ELP27, i.e., the stages of fast phenology succession (Fig. 2b).

In the present study, the phenological data of 35 years were allocated

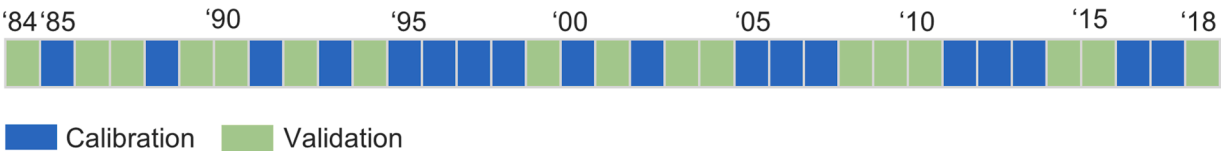

Fig. 3. Years of phenological observation data as allocated for calibration and validation.

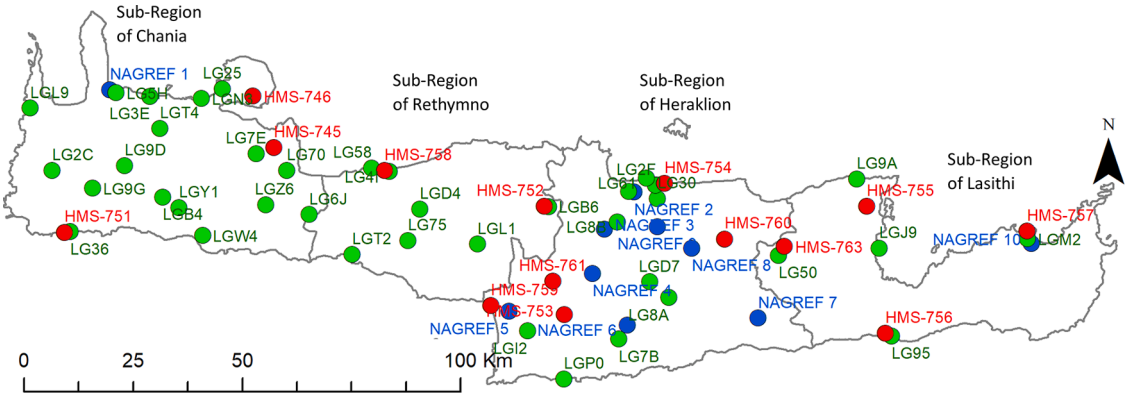

Fig. 4. Spatial distribution of the meteorological stations on the island of Crete. Red indicates the Hellenic Meteorological Service (HMS), blue indicates the NAGREF stations and green indicates the National Observatory of Athens network station (LG). Numbers following the initials for each station are part of the respective agency coding system.

randomly into two datasets for calibration and validation (Fig. 3).

3.3. Available temperature data

3.3.1. Observed temperature data

To determine the temperature for the 20 vineyard sites, daily temperature records from a total of 63 meteorological stations distributed across the whole of Crete were used. These stations consisted of (a) 14 stations of the Hellenic Meteorological Service (HMS), with an average of 36 years of records, ranging between 11 and 64 years between 1955 and 2019, (b) 10 stations of the National Agricultural Research Foundation (NAGREF) with a uniform recording period starting in 2007 or 2008 spanning 2019, and (c) 39 stations of the National Observatory of Athens (NOA) with an average recording period of 8 years, ranging between 2.5 and 14 years, between 2006 and 2019. The NAGREF network is affiliated with the Greek Ministry of Rural Development and Food and is operated by the Regional Center for Plant Protection and Phytosanitary Control of Heraklion. The NOA network, although with a limited record timespan, was very useful for the purposes of this study, as it contributes to a complete climatology picture for different areas of Crete. The spatial distribution of the three meteorological station networks is shown in Fig. 4. All these datasets were used to estimate the temperature time series for the 20 sites of interest. However, the detailed methodology is beyond the scope of the study. Therefore, a brief description of the methodology is provided here, while additional information is included in Appendix B. As a first step, the temperature data from the 63 stations were filled in for any gaps between 1979 and 2019 using the "single best estimator approach" (Eischeid et al., 2000; Hasanpour Kashani and Dinpashoh, 2012). An evaluation study of Shabalala et al. (2019) has shown that regression fill-in methods surpass other methods (arithmetic, averaging and various weighing approaches) for filling missing temperature values. Each missing value was filled in using a linear regression equation between the station with missing values and the best correlating station. When the best correlating station did not have a recorded temperature value for a specific date, the next most correlating station was used.

After the gap filling process, the temperature timeseries of the 20 phenology observation locations were estimated using multiple linear regression with interpolation of residuals. The general principles of this methodology are well established and used in the literature in acknowledged initiatives such as the E-OBS dataset (Cornes et al., 2018). This methodology is also recommended as a standard for the regionalization of climate information (Hennemuth et al., 2013). Generalized linear regression of the mean 31-day moving window, with the elevation and the distance from the seashore, provided the climatological temperature for each of the 20 locations. Then, the residuals between the climatological temperature for each station point and the actual temperature were estimated and interpolated to each point of interest. Six different interpolation methods were tested and validated, with the best results attained by inverse distance weighting. Details about the leave-one-out cross validation results are provided in Appendix B – Table B1 and Appendix B – Fig. B1. Finally, the residual temperature was added to the climatological temperature to provide the temperature estimation in each location of interest. The stations accessed in this study extend well beyond the spatial distribution of the 20 sites where the phenological observations were made, as the temperature database for the island of Crete was created to support research on viticulture as well as other crops spanning the whole island.

3.3.2. Projected regional climate model temperatures

Modeled daily temperature data were obtained from an ensemble of seven high-resolution (0.11°, ~x223C12.5 km) RCMs participating in the Coordinated Regional Downscaling Experiment for Europe initiative Euro-CORDEX 0.11° or EUR-11 (Jacob et al., 2013) as listed in Appendix Table A2. Two future representative concentration pathways (RCPs), RCP4.5 and RCP8.5 (Moss et al., 2010; O'Neill et al., 2014), were considered. These concentration trajectories describe different possible future climate periods with different volumes of emitted greenhouse gasses (GHGs). The RCPs are labeled based on the projected change in the total solar irradiance in 2100. The RCP 4.5 is a mid-range climate change scenario that describes a stabilization in the radiative forcings by 2100 (Wise et al., 2009) at approximately 4.5 W/m^2 by employing a range of technologies and strategies for reducing greenhouse gas emissions. RCP 8.5 is a high-end climate change scenario with radiative forcings increasing steadily until 2100 and beyond (Riahi et al., 2011), with an additional radiative forcing of 8.5 W/m^2 in 2100. This scenario

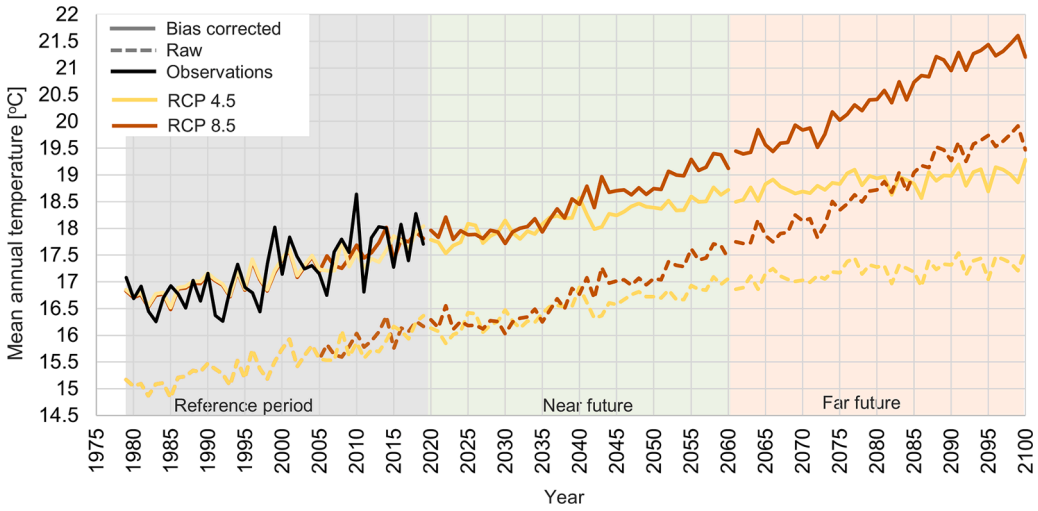

Fig. 5. Mean annual temperatures as an average across the 20 examined locations. The black line shows the mean annual observed temperatures, the dashed yellow line shows the raw RCP4.5, the dashed orange line shows the raw RCP8.5, the solid yellow line shows the bias-corrected RCP4.5, and the solid orange line shows the bias-corrected RCP8.5.

Table 2
Average, slope of the annual mean data (as shown in Fig. 5) and standard deviation of the daily values for the observed and EUR-11 CORDEX RCM data before and after the adjustment.

			Average [°C]	Slope [°C/year]	Standard Deviation [°C]
		Observed	17.2	0.035	6.2
RAW	RCP4.5	1979–2019	15.5	0.030	6.1
		2021–2060	16.5	0.024	6.2
		2061–2100	17.2	0.011	6.2
	RCP8.5	1979–2019	15.2	0.028	6.1
		2021–2060	16.8	0.041	6.3
		2061–2100	18.6	0.058	6.4
CORRECTED	RCP4.5	1979–2019	17.2	0.030	6.1
		2021–2060	18.2	0.024	6.2
		2061–2100	18.9	0.011	6.3
	RCP8.5	1979–2019	17.2	0.028	6.1
		2021–2060	18.8	0.041	6.4
		2061–2100	20.4	0.058	6.5

is referred to as 'business as usual', indicating that it may be the outcome if society does not take actions to reduce greenhouse gas emissions. A series of recent studies focusing on local or regional Mediterranean scales have used EUR-11 experiments for climate change impact assessments (Grillakis et al., 2020; Mascaro et al., 2018; Molina et al., 2020). The selection of the RCMs in the present study is similar to the selection performed in (Jacob et al., 2018) with a few modifications, i.e., exclusion of the HadGEM2-ES Global Climate Model (GCM)-driven simulation due to the 360 days-per-year calendar it uses, as well as the addition of three more model simulations. A complete list of the RCMs used is provided in Appendix Table A2. For the purposes of this study, the future temperatures of two forty-year periods, one in the near future (NF) (2021–2060) and one for the far future (FF) (2061–2100), were compared against the historical period of 1980–2019.

Raw climate model data quite often experience biases in the mean and the annual distribution in comparison to observations (Christensen et al., 2008; Haerter et al., 2011). To resolve this issue, the daily RCM temperature data were adjusted for their biases using the multisegment statistical bias correction (MSBC) quantile mapping methodology originally presented in (Grillakis et al., 2013) with the addition of the trend-preserving module presented in (Grillakis et al., 2017). This module allows for the long-term trend preservation of the temperature. The method considers different segments on the cumulative density function space and uses quantile mapping in each of the segments for the adjustment. This methodology belongs to the so-called parametric quantile mapping techniques. Advantages and drawbacks related to quantile mapping are discussed in Maraun et al. (2010) and Themeßl et al. (2012). The methodology considers stationarity of the data for the adjustment, i.e., the adjustment established in a calibration period can be applied to any time period within or outside the calibration time period. The methodology results have been compared to other methods in the Bias Correction Intercomparison Project (BCIP) (Nikulin et al., 2015). This methodology has already been previously used in the climate change impact study of (Nerantzaki et al., 2019) for the island of Crete.

The RCM data were interpolated to the 20 locations where phenological data were available using the nearest neighbor technique. The data were then bias adjusted towards the temperature observations of the 20 locations. For the adjustment, the reference period of 1979 to 2019 was used. As the EUR-11 historical simulation period ends in 2005, with 2006 onwards simulations to be forced by the RCP forcings, the bias adjustment was performed twice for the baseline period, once for the 1979–2005 complemented with the RCP4.5 between 2006 and 2019 and once complemented with RCP8.5 between 2006 and 2019 (Appendix Fig. A1).

4. Results

4.1. RCM temperature data bias adjustment

Temperature data were adjusted for biases, using as a reference the observed data from the period 1979–2019 (reference period). Fig. 5 presents the mean annual temperature as an average across the 20 examined locations before and after the adjustment. The RCM data exhibited a 1.7 °C–2 °C mean difference in the reference period (depending on the pathway to replenish the 2006–2019 data), also shown in Table 2. Raw and adjusted data exhibited a similar long-term trend, as expected by the trend-preserving adjustment methodology used. The RCM data, as shown in Fig. 5, exhibited a lower variation in comparison to the observations because of the 7 RCM data averaging.

Seasonal temperature analysis on the adjusted data revealed a nonuniform temperature change in the future projections (Fig. 6). The temperature increase is more intense in spring to summer months. In almost all analyzed periods and climate change scenarios, December was the month with the least warming, while June was the month with the highest warming. Specifically, for the near future period, RCP4.5

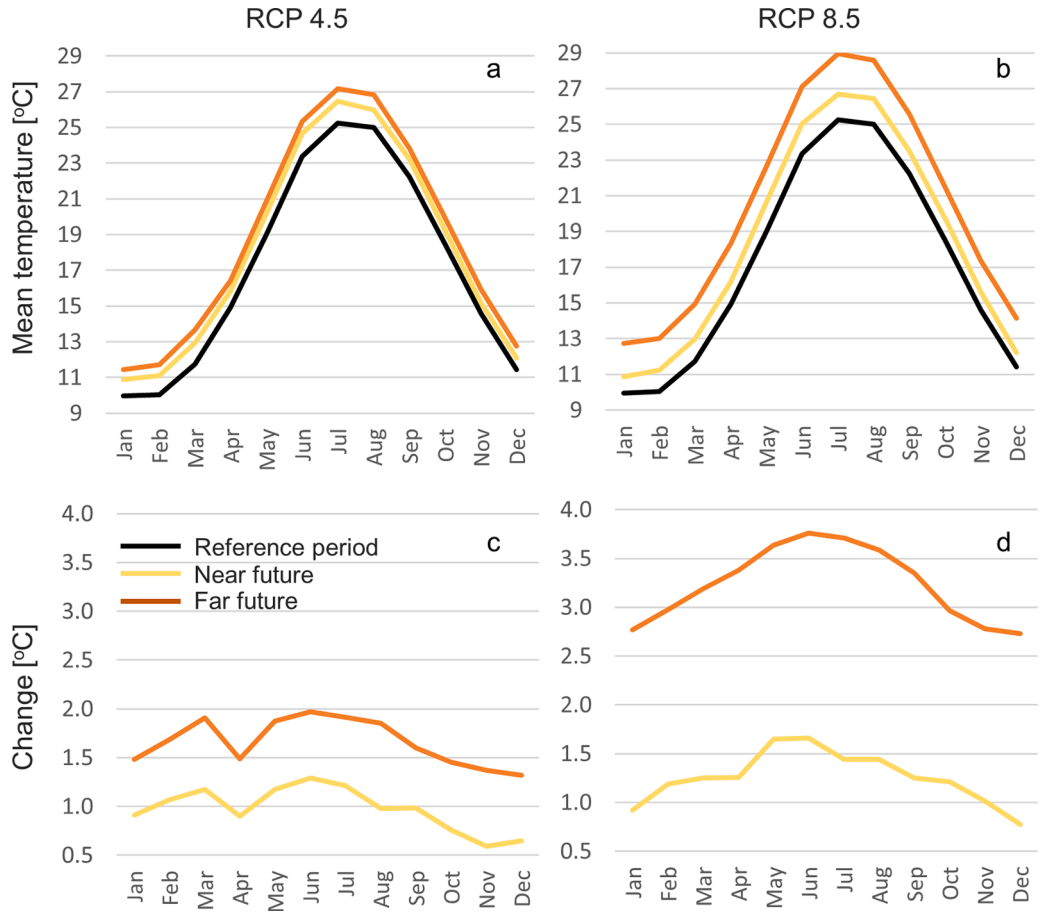

Fig. 6. Temperature seasonality as an average for each study period (reference, near future, far future), (a) for the RCP4.5 scenario and (b) for the RCP8.5 scenario. Change in temperature seasonality for the two future periods, (c) for RCP4.5 and (d) for RCP8.5.

Table 3
Optimized values for the analyzed parameters.

Parameter	Optimized value
Eq. (1), parameter Ph_{final}	40
Eq. (1), parameter k	0.0015
Eq. (1), parameter p	3.78
Eq. (2), parameter a	2.56
Eq. (2), parameter b	21.63
Eq. (2), parameter c	23.58
DoY	19

shows an increase between 0.6 °C (November) and 1.3 °C (June), while RCP8.5 shows a warming between 0.7 °C (December) and 1.3 °C (June). The respective changes for the far future period were projected to be between 1.3 °C (December) and 2 °C (June) for RCP4.5, while for RCP8.5, the respective increase is projected between 2.7 °C (January) and 3.8 °C (June).

4.2. Calibration and validation of the phenological model

The calibration procedure produced the optimized parameters shown in Table 3. In Fig. 7, the RMSD between the observed and calibrated ELP stages is shown as a function of different pairs of seven calibrated parameters. In a few couples of the parameters, there was a clear pattern between their variation and the RMSD, the clearest example being the variation of parameters a and k. Nevertheless, most couples present a nearly random RMSD pattern. This confirmed that none of the 7 parameters optimized against the RMSD were redundant.

The optimization procedure provided an overall RMSD of 8.7 days and an RMSD of 2.77 on the ELP scale. The respective validation error, estimated on the validation data, equaled RMSD 8.6 days and 2.79 ELP scale units. The R^2 values between the observations and the simulation were 0.93 and 0.92, respectively. In Table 4, the RMSD for the different developmental stages was provided for the calibration, validation, and combined data, both in time difference and ELP units. As a result, the model exhibited good overall performance. The model showed the lowest RMSD for the flowering and maturing stages, while the highest difference was found for the shoot development stages. The maturing stages (ELP 37 or higher) show an overall RMSD of 6.6 days. In Fig. 8, the simulation results for four of the studied locations are shown, for 2017 that was included in the calibration and for 2018 that was included in the validation procedure. The RMSD results shown in Table 4 are similar, indicating the suitability of the model for use with other data. A scatter plot of the observed and the simulated day of occurrence for each phenological observation is provided in the Appendix, Fig. A2. Mean Absolute Error (MAE) and the Agreement Index are also provided. A sensitivity analysis was performed to validate the optimal calibration point of the genetic algorithm (Appendix Fig. A3).

4.3. Effects of future temperatures on the growing degree day accumulation

Increasing temperatures are expected to affect changes in the growing degree days accumulated during the growing season. In Fig. 9a, the average simulated temperatures from February to September are shown for the near and far future periods. The effect of the temperature change was expressed in the accumulated GDDs, as shown in Fig. 9b. In the near future, GDD accumulation will be nearly identical between the

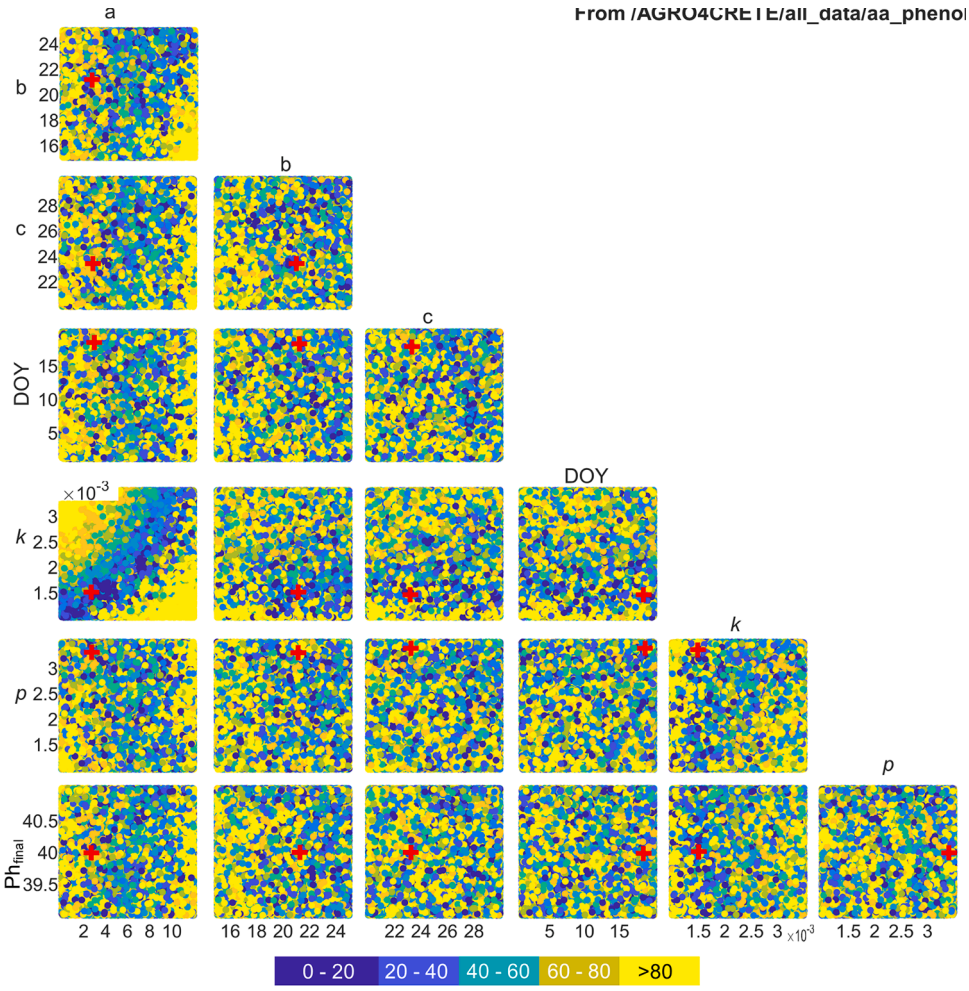

Fig. 7. RMSD of the calibration procedure as a function of different pairs of calibrated parameters. Red crosses represent the optimized values.

Table 4
Calibration, validation and all period RMSD for different development stages in days and, in parentheses, ELP scale units.

Stage (ELP scale)	RMSD calibration	RMSD validation	Overall RMSD
All stages (4–38)	8.7 (2.77)	8.6 (2.79)	8.7 (2.78)
Budbreak (4–5)	8.49 (1.58)	8.83 (1.57)	8.67 (1.58)
Shoot development (5–18)	10.03 (3.34)	10.57 (3.35)	10.33 (3.35)
Flowering (19–26)	5.43 (1.81)	6.66 (2.17)	6.19 (2.03)
Berry development (27–33)	7.83 (1.95)	7.07 (1.71)	7.48 (1.84)
Ripening (34–38)	11.56 (1.02)	10.28 (0.74)	10.75 (0.84)
Maturing (>37)	6.60 (0.66)	6.83 (0.57)	6.75 (0.57)

two pathways, RCP4.5 and RCP8.5, while in the far future, the two pathways will be well discernible. RCP4.5 was close to the near future GDD accumulation, while RCP8.5 shows faster GDD accumulation. In both pathways and periods, GDD accumulation appears to converge to similar values in early August. These different patterns of GDD accumulation are also shown in Fig. 9c, where the average degree day gain was shown for each month. For the historical period, degree day accumulation increases until June. Thereafter, it remained constant due to the increase in temperatures to values beyond the level of linear increase (calibrated at 21.6 °C) or the heat threshold (calibrated at 23.6 °C), beyond which plant development slows down. For the projection periods, the degree day accumulation in the spring was enhanced by the increasing temperatures until June (May for far future for RCP8.5). During the summer months, a significant slowdown of GDD accumulation was observed.

4.4. Future temperature effects on vine phenology

The calibrated phenological model was used to simulate the phenological stages of two future periods under the two RCP pathways. In Fig. 10, the representation of five phenological periods is shown for the historical and examined future periods and pathways. In the near future, the start of budburst was expected to be advanced by 6 and 7 days for RCP4.5 and RCP8.5, respectively. The end of the ripening period was expected to be advanced by 3 days for both pathways. For the far future period, the projections revealed a significant advancement for the start of budburst by 10 and 16 days for RCP4.5 and RCP8.5, respectively. The end of the ripening period was expected to be advanced by 4 and 5 days, respectively. Table 5 shows the DoY where each phenological phase starts and ends, the changes for NF and FF periods and the two pathways examined in relation to the historical period, and the length of each phenophase period. These results indicate that while there was an overall advancement in the phenophase start and end between budburst and berry development, their total length was not expected to change. The ripening phase exhibits an increasing trend by up to 4 days for the near future pathways and by 6 to 12 days for the far future for RCP4.5 and RCP8.5.

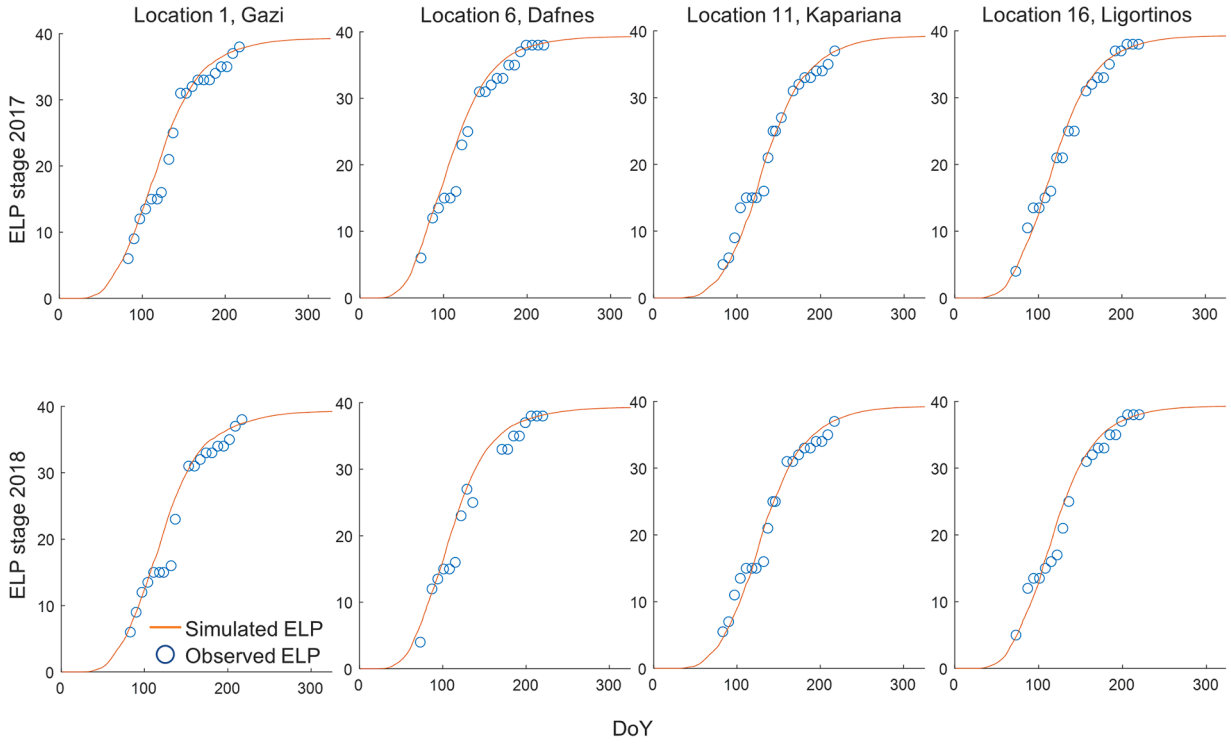

Fig. 8. Example of calibration and validation results from four locations. The 2017 growing season (upper) contributed to the calibration data, and the 2018 season (lower) contributed to the validation data. Red lines and blue circles correspond to the simulated and observed ELP stages, respectively.

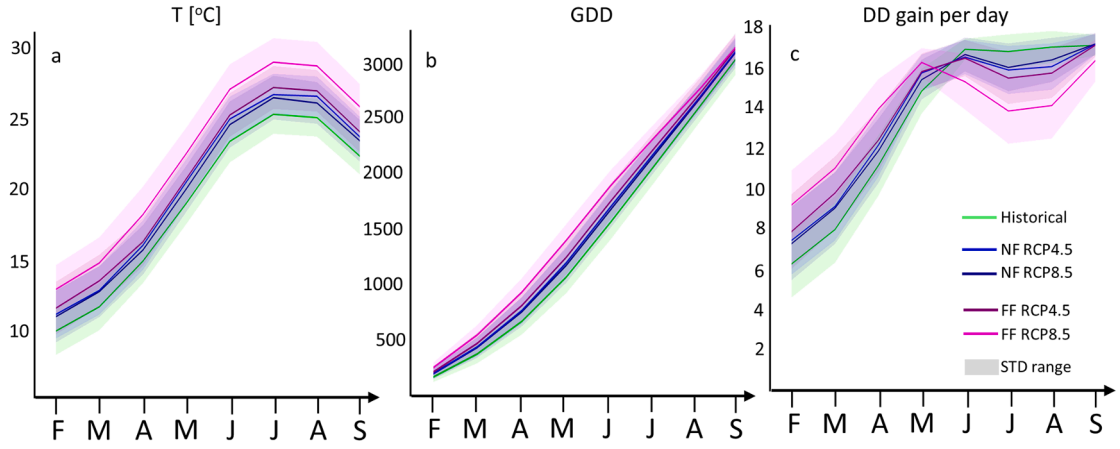

Fig. 9. Expected changes in growing degree day accumulation due to increasing temperatures. (a) Mean daily temperature across all RCMs and study locations, from February to September. Different colors depict the different scenarios and periods studied. The shaded areas depict the standard deviation range. (b) The same as (a) but for the GDD accumulation. (c) The mean daily degree day accumulation for each month. NF = near future, FF = far future, STD = standard deviation.

5. Discussion

In this study, a phenological model was calibrated and validated based on long records of temperatures and phenological observations of the grapevine cultivar "Sultana". The model was used to estimate future shifts in grapevine phenological stages under two climate pathways and two future periods.

The calibrated phenology model indicated that there is a strong nonlinear correlation between the ELP phenological scale and the accumulated GDDs estimated by the three-parameter model, i.e., base, upper and heat threshold temperatures. The calibration-validation RMS difference was estimated between 5.4 and 11.5 days, depending on the phenological stage, with the model best fitting in the flowering and maturing stage prediction. The average RMSD was calculated at 8.6 days, close to the estimated advancement in the near future phenology shifts for both pathways. These values were similar to those reported by Zapata et al. (2015), who obtained an RMSD ranging between 6.1 and 10.8 days for the grapevine cultivars Merlot, Cabernet Sauvignon and Chardonnay. The aforementioned RMSD range found in this study was lower than that found by Verdugo-Vásquez et al. (2017), who reported RMSD values between 4.4 and 19.4 days for table grapes, although their model initiated the prediction at budbreak (i.e., a fixed phenological event) instead of a fixed day of the year as a start counting GDDs (the case in this study). Parker et al. (2011) used a fixed DoY (60th) to build a multicultivar model that predicts the stages from flowering to veraison. Their results indicated RMS differences between 1.8 and 4.7 days,

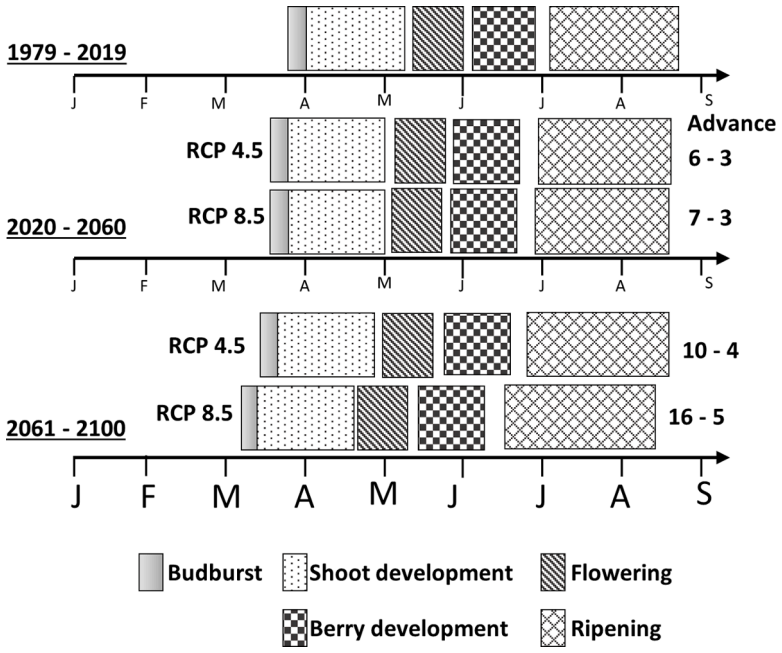

Fig. 10. Simulated phenological phases in the historical and two future projected periods for the two pathways studied. On the right side of the figure, the advance (in days) at the start of the budburst and at the end of the maturity stage is shown.

Table 5
Changes in the start and end of the different phenophases, depicted as the day of the year, and phenophase length. These results were calculated as the average of the different RCM model results. NF = Near Future, FF = Far Future.

Stage:		Budburst		Shoot development		Flowering		Berry Development		Ripening	
DoY		From	To	From	To	From	To	From	To	From	To
Historical Period		86	92	93	131	135	154	158	184	192	240
NF	RCP4.5	80 (−6)	86 (−6)	87 (−6)	124 (−7)	128 (−7)	148 (−6)	152 (−6)	178 (−6)	186 (−6)	237 (−3)
	RCP8.5	79 (−7)	85 (−7)	86 (−7)	123 (−8)	127 (−8)	146 (−8)	151 (−7)	177 (−7)	185 (−7)	237 (−3)
FF	RCP4.5	76 (−10)	82 (−10)	83 (−10)	120 (−11)	124 (−11)	143 (−11)	148 (−10)	174 (−10)	182 (−10)	236 (−4)
	RCP8.5	70 (−16)	75 (−17)	76 (−17)	112 (−19)	115 (−20)	135 (−19)	139 (−19)	167 (−17)	175 (−17)	235 (−5)
Phenophase length											
Historical Period		6		38		19		26		48	
NF	RCP4.5	6		37		20		26		51	
	RCP8.5	6		37		19		26		52	
FF	RCP4.5	6		37		19		26		54	
	RCP8.5	5		36		20		28		60	

Table A1
Observation locations. Geographical data and numbers of phenological observations. HTRS: Hellenic Terrestrial Reference System.

	Location name	HTRS X	HTRS Y	Elevation	Number of observations
1	Gazi	595,814	3,908,818	25.5	500
2	Voutes	596,213	3,903,089	234	310
3	Kasteli	621,822	3,896,907	340	188
4	Pentamodi	593,401	3,901,108	327	118
5	Pyrgou	592,723	3,898,265	400	157
6	Dafnes	596,134	3,897,813	349	280
7	Profitis Ilias	600,088	3,897,124	350	15
8	Ano Asites	591,022	3,894,778	480	47
9	Gkagkales	592,173	3,880,095	245	32
10	Agia Varvara	591,020	3,888,702	612	122
11	Kapariana	581,285	3,877,044	65	122
12	Vagionia	591,686	3,873,392	245	44
13	Episkopi	612,613	3,902,295	269	15
14	Mesochorio	610,222	3,875,329	307	87
15	Kasteliana	614,644	3,877,229	316	41
16	Ligortinos	606,878	3,882,217	402	27
17	Damasta	583,893	3,912,628	420	14
18	Alagni	611,310	3,893,617	422	85
19	Choumeri	613,833	3,891,677	355	15
20	Archanes	605,828	3,900,673	367	23

Table A2
List of the EURO CORDEX Regional Climate Models (RCMs), their driving Global Climate Models (GCMs) used in this study. Also, key references are provided.

Driving GCM	RCM	Key refs.
EC-EARTH	KNMI-RACMO22E	Van Meijgaard et al. (2012)
EC-EARTH	SMHI-RCA4	Kjellström et al. (2016)
IPSL-CM5A-MR	IPSL-INERIS-WRF331F	Skamarock and Klemp (2008)
MPI-ESM-LR	CSC-REMO	Jacob et al. (2012)
CNRM-CM5	SMHI-RCA4	Kjellström et al. (2016)
EC-EARTH	DMI-HIRHAM5	Christensen et al. (2007)
MPI-ESM-LR	SMHI-RCA4	Kjellström et al. (2016)

depending on the cultivar tested. The key difference from the model developed in the present work was that this study approximates all the phenology stages from budbreak to maturity, which widens its usefulness, although it has a cost in the fitting performance. According to Molitor et al. (2014), the use of a starting date based on budbreak makes the model more robust. It is still worth noting that the results of this study should be interpreted with caution regarding the near future projections, as the estimated changes in the phenology timing are, roughly, at the same range as the uncertainty related to the model calibration error.

Table A3
Calibration (CAL), validation (VAL) and total (ALL) period Mean Absolute Error (MAE) and Agreement Index for each phenophase and for the entire cultivation season.

PHENOPHASES	MAE			AGREEMENT INDEX		
	CAL	VAL	ALL	CAL	VAL	ALL
All stages (4–38)	6.91	7.47	7.20	0.82	0.79	0.81
Budbreak (4–5)	8.38	8.70	8.56	0.89	0.88	0.88
Shoot development (5–18)	4.54	5.12	4.89	0.92	0.88	0.90
Flowering (19–26)	6.32	5.51	5.94	0.91	0.89	0.90
Berry development (27–33)	10.36	8.66	9.25	0.81	0.88	0.86
Ripening (34–38)	7.48	7.62	7.56	0.98	0.98	0.98

Our findings show that veraison, the onset of the ripening process, is predicted to be advanced by 6–17 days at all sites (Table 5), with the mean temperature during the 51–60 days following veraison (within July and August) being projected to increase by 3.8 °C. Changes in the phenology of several grapevine cultivars have also been found by other researchers during recent decades and under future climate conditions in connection to temperature increases. Jones and colleagues (2005) found that budbreak, flowering and veraison stages have advanced significantly over the last 50 years. Gate and Brisson (2010) estimated that flowering will advance by 8 days and veraison by 10 days in France for every Celsius temperature degree increase. García de Cortázar-Atauri and colleagues (2017) found a change in all phenological stages, by 15 to 30 days depending on the pathway, the cultivar and the region, up to 2100. Fraga and colleagues (2016b) reported that in northern Italy, phenological events under the RCP8.5 pathway could occur more than 30 days earlier. The results of these studies indicate an advancement in grapevine key phenological stages in the last few decades. They also indicate that an increasing trend in this advancement is expected in the future, according to projected warming scenarios.

The findings of this study indicate that while future temperatures are expected to increase more in the summer months (Figs. 6 and 9), it is shown that the GDD accumulation is stronger in the spring, with a degree day accumulation slowdown in the summer (Fig. 9), especially in the far future period of RCP8.5. The projected changes report a stronger trend for advancement of the early phenological stages, whereas this advancement is decreased in the later stages near maturation (Table 5). It may be worth investigating whether any lengthening of the cultivation period is likely to have significant implications in cropping systems. More inputs may be required, e.g., for plant protection and irrigation. These factors may have an impact on the profit margins and hence on the competitiveness of the cultivar grown in an area. On the other hand, a potential earlier production reaching the markets could compensate for the economic loss from higher production costs.

An issue to be addressed is the uneven distribution of the observations through the growing season and through the years for which the model was calibrated and validated. The uneven distribution of phenological observations may have induced a bias in the phenological model that may partly explain the differences in the RMS for the different phenological stages (Table 4). Other systematic changes that were not taken into consideration, as there were no records, are cultivation practices (e.g., irrigation, fertilization, pruning). Additionally, no data were available on the vine training systems and different rootstock-scion combinations. Another limitation of this study is that the phenological model considers only the temperature parameter, while there is significant literature that highlights the importance of other climatic parameters, such as precipitation. Additionally, the model validation was subject to the accuracy of the temperature and phenology

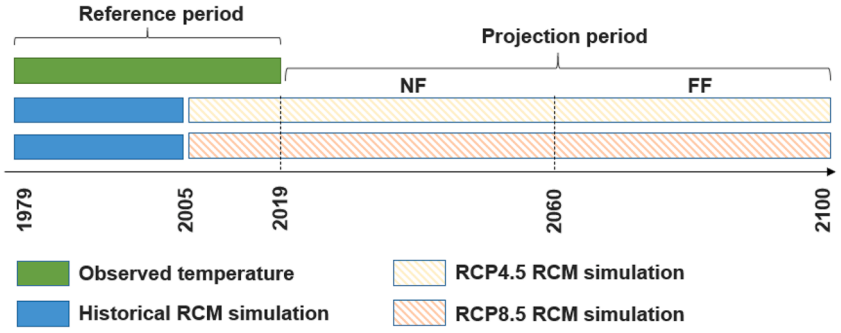

Fig. A1. Schematic representation of the different period definitions used in the study. The reference period coincides with the temperature data observations period. The Regional Climate Model (RCM) simulations under the Representative Concentrations Pathways (RCPs) 4.5 and 8.5 are also shown. The Near and Far Future periods of the projections are referred as NF and FF, respectively.

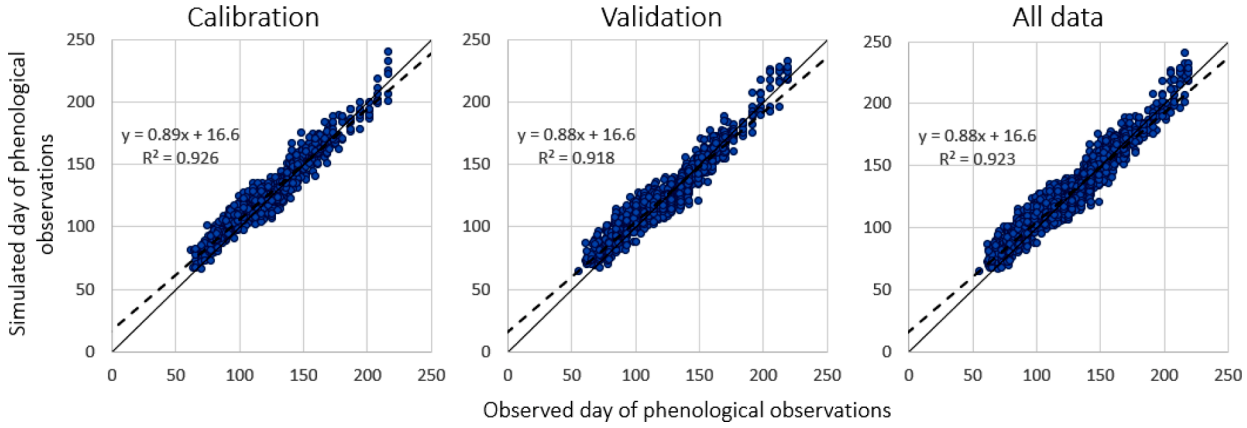

Fig. A2. Scatter plot between the day of the year that each phenology observation was recorded and the respective simulated day of the year, for the calibration, validation and the entire dataset.

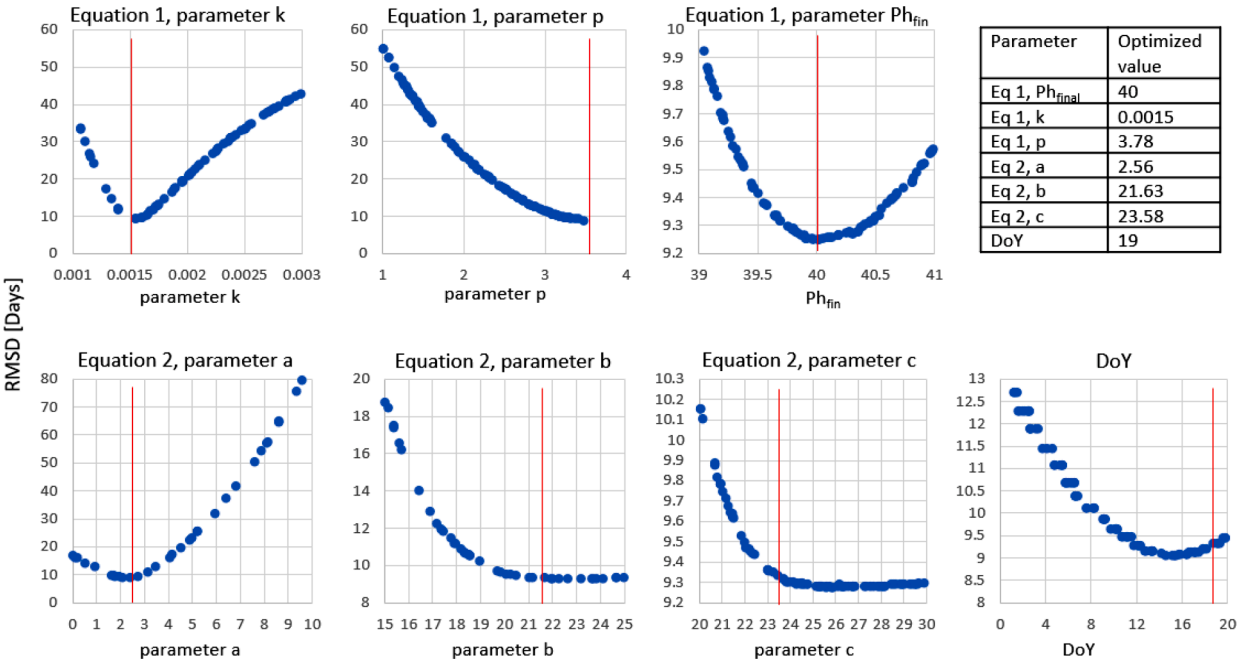

Parameter	Optimized value
Eq 1, Ph_{final}	40
Eq 1, k	0.0015
Eq 1, p	3.78
Eq 2, a	2.56
Eq 2, b	21.63
Eq 2, c	23.58
DoY	19

Fig. A3. Sensitivity analysis of the 7 optimized variables. For each variable tested, the other six variables were kept constant to the genetic algorithm's optimized value (shown in the table in the top right corner).

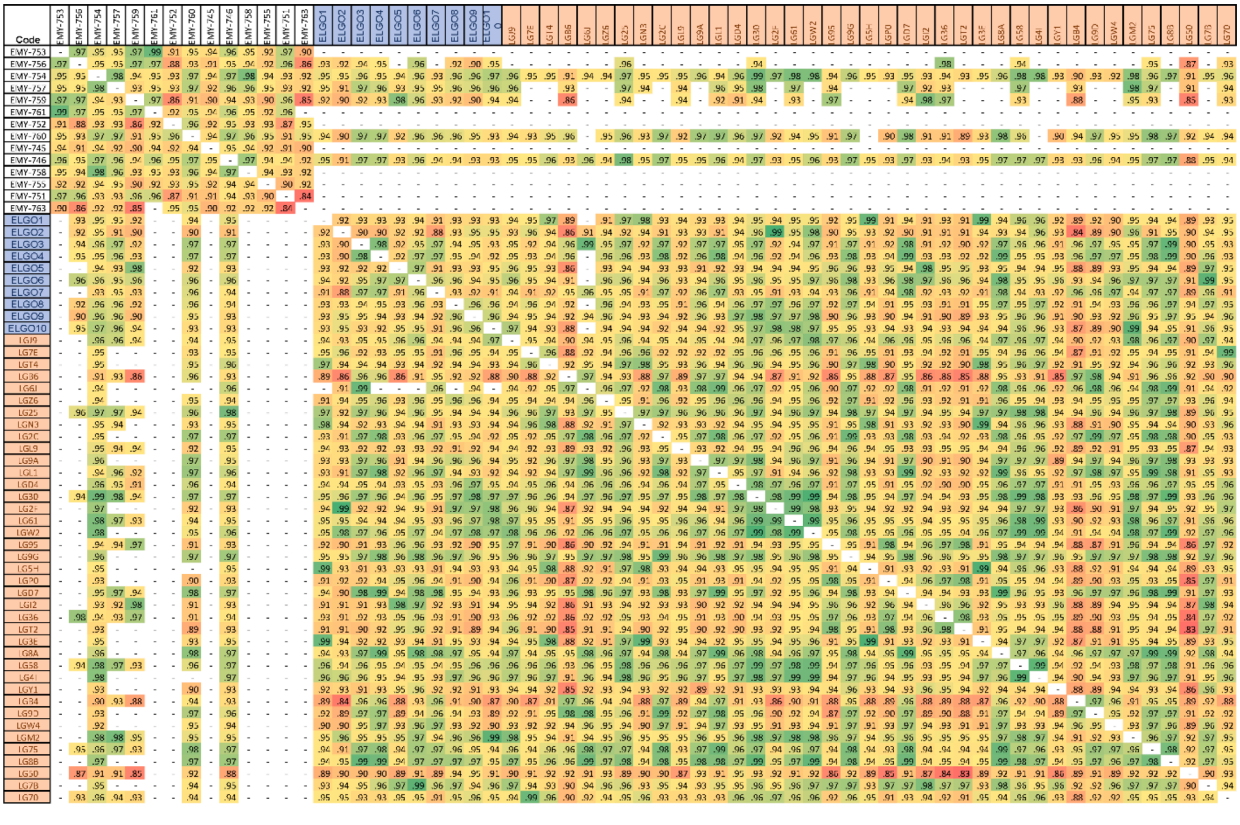

Fig. B1. Comparison of different interpolation methods. Box plots encompass the results among the different stations. The different box plots provide information for Triangulation-based linear interpolation (blue), Triangulation-based nearest neighbor interpolation (orange), Triangulation-based natural neighbor interpolation (gray), cubic interpolation (yellow), Biharmonic spline interpolation (pale blue) and inverse distance weighting (green), respectively. Panel (a) Root mean square error, (b) the difference between the observations and the estimation (estimation - observations), (c) the standard deviation of the difference and (d) the ratio of the simulated over the observed variance.

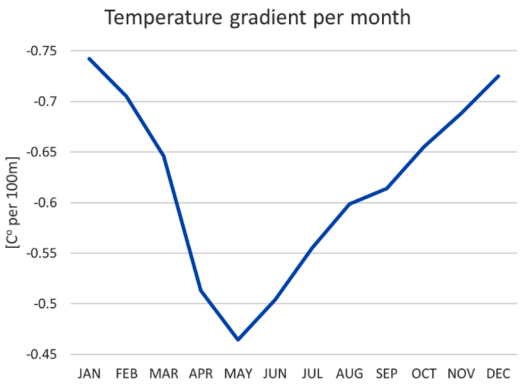

Fig. B2. Symmetrical matrix with the correlation coefficients [R^2] between each pair of stations. Empty cells indicate station pairs with less than two years of concurrent temperature recordings.

observations. Finally, the potential effects of changes in CO_2 concentration or potential impacts from known phytotoxic increases in tropospheric ozone concentrations were not taken into consideration.

During grape ripening, berries undergo major changes in acidity, anthocyanin accumulation and terpenol formation (Duchêne et al., 2012). It is generally accepted that the highest grape quality is obtained when grapes ripen neither too early nor too late in the season and that elevated temperatures can impair grape quality parameters. Since the maturation of grapes is likely to occur under increasing temperatures in the future due to projected advances in phenology, vine growing regions are expected to face abscission of grape berries, partial or total failure of flavor ripening, skin discoloration and absence of floral aromas (Jones et al., 2005). The model could be a helpful tool in designing adaptable management strategies against the effects of climate change or could potentially be used, along with seasonal temperature forecasts, for agricultural management or grape market forecasts. Seasonal forecasts have already shown their value for a 1- to 3-month range for the island of Crete (Grillakis et al., 2018).

The model developed in this study obtained satisfactory results in predicting the phenological phases of the Sultana cultivar. The best estimates were obtained for the prediction of maturity timing. The considerable shifts in grapevine timing reported in this study could alter the suitability of many vineyard regions today for profitable grape production, in other areas of Greece and in other countries where Sultana is grown as well as for other grapevine cultivars using a similar approach. A need for adaptations arises, e.g., the replacement of current cultivars with others of a later ripening period and/or a spatial shift of grapevine cultivation to cooler areas. In line with the findings of this and other studies mentioned above, appropriate adaptation strategies are already under evaluation. In this context, the combination of grapevine phenological models with climate change projections constitutes a valuable tool for restructuring sustainable viticultural production systems.

6. Conclusions

The application of the model developed in this study to future projected climate conditions produced three significant findings: (1) the expected earlier emergence of the different phenophases, from budbreak to berry development, in grapevines, (2) the lengthening of the ripening period and (3) there were no noticeable changes in the duration of the cultivation period, although there was a significant advancement in the

Table B1
Average results from all stations.

	linear	nearest	natural	cubic	v4	IDW
RMSE	1.35	1.54	1.29	1.42	1.58	1.39
Difference	0.060	−0.058	0.080	−0.005	−0.026	0.001
STD of the difference	1.04	1.20	1.02	1.09	1.23	1.16
Fraction of variance	0.98	1.00	0.98	0.99	1.01	0.96

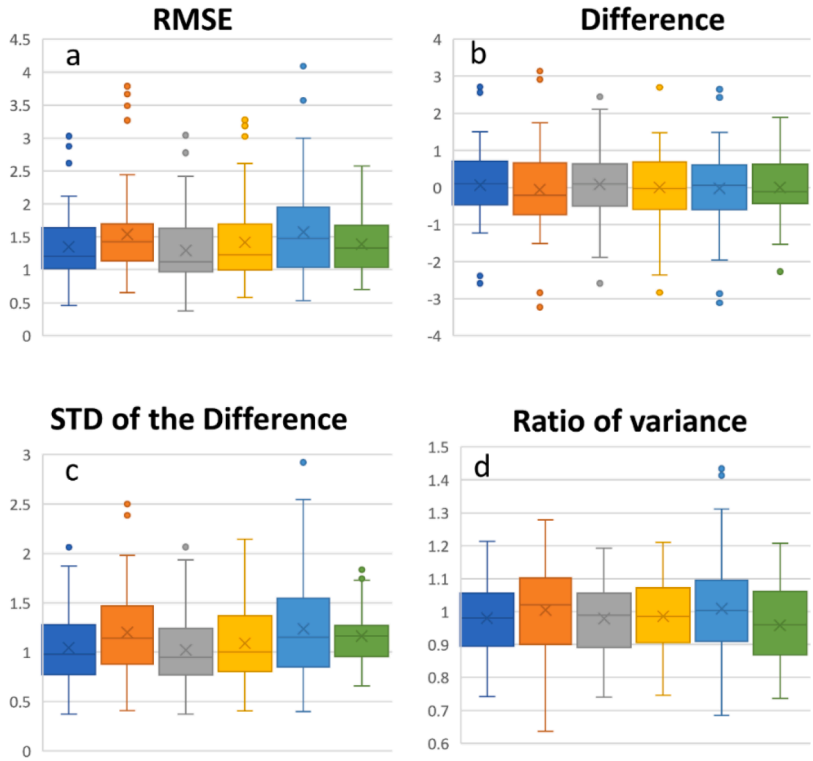

Fig. B3. Average temperature gradient per 100 m for each calendar month for the island of Crete.

day of the year for the harvest. These conclusions lend support to current efforts for climate change adaptation strategies for viticulture.

Declaration of Competing Interest

The authors declare that they have no known competing financial interests or personal relationships that could have appeared to influence the work reported in this paper.

Authors have no competing interests to declare.

Acknowledgments

We acknowledge the research program Agro4Crete funded by Greek General Secretariat for Research and Technology.

We acknowledge (a) Hellenic National Meteorological Service, (b) National Agricultural Research Foundation and (c) National Observatory of Athens, for the provision of the meteorological data used in this study.

We would like to thank the agronomists of the Regional Center for Plant Protection and Phytosanitary Control of Heraklion, Maria Roditaki and Nikolaos Bagis for their valuable collaboration and for the provision of the phenological and part of the meteorological data.

Appendix section A

Table A1–Table A3
Fig. A1–Fig. A3.

Appendix section B

(a) Temporal fill-in at a station level

Initially, all the stations were tested for their correlation in the temperature in the form of R^2. A threshold of at least two years of concurrent temperature recordings was applied for the R^2 estimation. Wherever the available concurrent recordings between two stations were less than 2 years, the correlation was omitted. The correlations are shown in Fig. B2.

Each missing value in each station is filled in using a unique linear interpolation equation between the missing value station and the best correlating one. If the best correlating station does not have a temperature value for the specific missing value date, the next most correlating station is used.

(b) Spatial interpolation at the 20 sites of interest

After the temporal fill-in, the spatial interpolation at the 20 sites of interest was performed using the linear regression with interpolation of residuals (Cornes et al., 2018; Hennemuth et al., 2013). Due to the high orography of the island, the correlation of the temperature and the altitude was estimated at a moving 31-day window for the 365 calendar days of the year. For illustration purposes, Fig. B3 shows the temperature-elevation gradient for each calendar month.

Additionally, a range of - other than elevation - temperature regression predictors were assessed for their ability to correlate to the temperature. Linear regression models were constructed between temperature and latitude, longitude, distance from the shore and terrain slope. It was found that beyond the elevation, only the distance from the shore provided a significant correlation at a 95% confidence level. Hence, only elevation and the distance from the shoreline were used in the Generalized linear regression model to obtain the correlation between elevation, distance from the shore and the moving 31-day window temperature as a predictant. It is worth mentioning that the combined use of those two variables in the regression model provided smaller Akaike's Information Criterion (AIC) comparing to the AIC of a linear model using each individual variable, indicating that their combination increases the information that the linear model provides, with a reasonable tradeoff increase of the model complexity. The established linear equations for each calendar day were used to estimate the climatological temperature for each one of the 20 locations of interest, using their elevation and their distance from the shore.

(c) Temperature residual interpolations

Following the methods of Cornes et al. (2018) and Hennemuth et al. (2013), a series of different interpolation methods were assessed for the residual interpolation. These methods were tested and validated using a Leave-one-out-cross validation (LOOC). The methods tested were Triangulation-based linear interpolation, Triangulation-based nearest neighbor interpolation, Triangulation-based natural neighbor interpolation, cubic interpolation, Biharmonic spline interpolation and inverse distance weighting. Comparison of the different methods is provided in the Fig. B4. Each box plot encompasses the results for the different stations for the leave one out test. Hence all stations were left once outside as a validation while the estimation of the temperature time series was repeated using all the these stations. The results are shown for Triangulation-based linear interpolation, Triangulation-based nearest neighbor interpolation, Triangulation-based natural neighbor interpolation, cubic interpolation, Biharmonic spline interpolation and inverse distance weighting (IDW), respectively. Linear triangulation, natural neighbor triangulation and cubic interpolation could not estimate the leave one out test for the stations that were not included in triangle spatially, hence 9 stations estimations were not included in the results, while also this was a barrier on selecting those methods for the spatial interpolation. The mean values of the above box plots are also shown in Table B1. Among the three methods that can spatially extrapolate the residuals, the best performing was the IDW, which presented the lowest RMSE, average difference and standard deviation of the difference. The results are comparable with those of datasets built for other countries, e.g. the STEAD dataset for Spain (Serrano-Notivoli et al., 2019).

Appendix references

Cornes, R.C., van der Schrier, G., van den Besselaar, E.J.M., Jones, P. D., 2018. An ensemble version of the E-OBS temperature and precipitation data sets. J. Geophys. Res. Atmos. 123, 9391–9409.

Hennemuth, B., Bender, S., Bülow, K., Dreier, N., Keup-Thiel, E., Krüger, O., Mudersbach, C., Radermacher, C., Schoetter, R., 2013. Statistical methods for the analysis of simulated and observed climate data: applied in projects and institutions dealing with climate change impact and adaptation. CSC Report 13, Climate Service Center, Germany.

Serrano-Notivoli, R., Beguería, S., De Luis, M., 2019. STEAD: A high-resolution daily gridded temperature dataset for Spain. Earth Syst. Sci. Data 11, 1171–1188. 10.5194/ESSD-11-1171-2019.

References

Baggiolini, M., 1952. Les stages repères dans le développement annuel de la vigne et leur utilisation pratique. Rev. Rom. Agric. Vitic. 8 (1), 4–6.

Baillod, M., Baggiolini, M., 1993. Les stades repères de la vigne. Rev. Suisse Vitic. Arboric. Hortic. 25, 7–9.

Breitfeld, M.G., Shanno, D.F., 1995. A Globally Convergent Penalty-Barrier Algorithm For Nonlinear Programming. Springer, Berlin, Heidelberg, pp. 22–27. https://doi.org/10.1007/978-3-642-79459-9_5.

Chartzoulakis, K., 2001. Water resources management in the Island of Crete, Greece, with emphasis on the agricultural use. Water Policy 3, 193–205. https://doi.org/10.1016/S1366-7017(01)00012-5.

Christensen, J.H., Boberg, F., Christensen, O.B., Lucas-Picher, P., 2008. On the need for bias correction of regional climate change projections of temperature and precipitation. Geophys. Res. Lett. 35, L20709. https://doi.org/10.1029/2008GL035694.

Conn, A.R., Gould, N.I.M., Toint, P.L., 1991. Globally convergent augmented Lagrangian algorithm for optimization with general constraints and simple bounds. SIAM J. Numer. Anal. 28, 545–572. https://doi.org/10.1137/0728030.

Coombe, B.G., 1995. Growth stages of the Grapevine: adoption of a system for identifying grapevine growth stages. Aust. J. Grape Wine Res. 1, 104–110. https://doi.org/10.1111/j.1755-0238.1995.tb00086.x.
Cornes, R.C., van der Schrier, G., van den Besselaar, E.J.M., Jones, P.D., 2018. An ensemble version of the E-OBS temperature and precipitation data sets. J. Geophys. Res. Atmos. 123, 9391–9409.
De Ollas, C., Morillón, R., Fotopoulos, V., Puértolas, J., Ollitrault, P., Gómez-Cadenas, A., Arbona, V., 2019. Facing climate change: biotechnology of iconic Mediterranean woody crops. Front. Plant Sci. 10.
Doupis, G., Chartzoulakis, K.S., Taskos, D., Patakas, A., 2020. The effects of drought and lemental UV-B radiation on physiological and biochemical traits of the grapevine cultivar "Soultanina. OENO One 54, 687–698. https://doi.org/10.20870/OENO-ONE.2020.54.4.3581.
Duchêne, E., Butterlin, G., Dumas, V., Merdinoglu, D., 2012. Towards the adaptation of grapevine varieties to climate change: QTLs and candidate genes for developmental stages. Theor. Appl. Genet. 124, 623–635. https://doi.org/10.1007/S00122-011-1734-1.
Duchene, E., Schneider, C., 2005. Grapevine and climatic changes: a glance at the situation in Alsace. Agron. Sustain. Dev. 25, 93–99. https://doi.org/10.1051/agro:2004057.
EC, 2020. Region of kriti - internal market, industry, entrepreneurship and SMEs - European commission [WWW Document]. URL https://ec.europa.eu/growth/tools-databases/regional-innovation-monitor/base-profile/region-kriti (accessed 2.9.20).
Eichhorn, K.W., Lorenz, D.H., 1977. Phänologische Entwicklungsstadien der Rebe | Nachrichtenblatt des Deutschen Pflanzenschutzdienstes [WWW Document]. URL https://ojs.openagrar.de/index.php/NachrichtenblattDPD/article/view/9586 (accessed 7.29.20).
Eischeid, J.K., Pasteris, P.A., Diaz, H.F., Plantico, M.S., Lott, N.J., 2000. Creating a serially complete, national daily time series of temperature and precipitation for the western United States. J. Appl. Meteorol. 39, 1580–1591, 10.1175/1520-0450(2000)039<1580:CASCND>2.0.CO;2.
Fernández-González, M., Rodríguez-Rajo, F.J., Escuredo, O., Aira, M.J., 2013. Influence of thermal requirement in the aerobiological and phenological behavior of two grapevine varieties. Aerobiologia 29, 523–535. https://doi.org/10.1007/s10453-013-9302-6 (Bologna).
Fraga, H., Santos, J.A., Malheiro, A.C., Oliveira, A.A., Moutinho-Pereira, J., Jones, G.V., 2016a. Climatic suitability of Portuguese grapevine varieties and climate change adaptation. Int. J. Climatol. 36, 1–12. https://doi.org/10.1002/joc.4325.
Fraga, H., Santos, J.A., Moutinho-Pereira, J., Carlos, C., Silvestre, J., Eiras-Dias, J., Mota, T., Malheiro, A.C., 2016b. Statistical modelling of grapevine phenology in Portuguese wine regions: observed trends and climate change projections. J. Agric. Sci. 154, 795–811. https://doi.org/10.1017/S0021859615000933.
García de Cortázar-Atauri, I., Duchêne, E., Destrac-Irvine, A., Barbeau, G., De Rességuier, L., Lacombe, T., Parker, A.K., Saurin, N., Van Leeuwen, C., 2017. Grapevine phenology in France: from past observations to future evolutions in the context of climate change. OENO One 51, 115. https://doi.org/10.20870/oeno-one.2016.0.0.1622.
Garcia de Cortazar Atauri, I., 2006. Adaptation du modèle STICS à la vigne (Vitis vinifera L.): utilisation dans le cadre d'une étude d'impact du changement climatique à l'échelle de la France.
Gate, P., Brisson, N., 2010. Advancement of phenological stages and shortening of phases. Climate change, agriculture and forests in France: simulations of the impacts main species. Green B. Clim. Proj. (2007–2010). ADEME, Angers, Fr. 65–78.
Giorgi, F., Lionello, P., 2008. Climate change projections for the Mediterranean region. Glob. Planet. Change 63, 90–104. https://doi.org/10.1016/j.gloplacha.2007.09.005.
Goldberg, D.E., 1989. Genetic Algorithms in Search, Optimization & Machine Learning. Addison-Wesley, Reading, Mass, p. p. 126.
Gordo, O., Sanz, J.J., 2010. Impact of climate change on plant phenology in Mediterranean ecosystems. Glob. Chang. Biol. 16, 1082–1106. https://doi.org/10.1111/j.1365-2486.2009.02084.x.
Grillakis, M., Koutroulis, A., Tsanis, I., 2018. Improving seasonal forecasts for basin scale hydrological applications. Water 10, 1593. https://doi.org/10.3390/w10111593.
Grillakis, M.G., Koutroulis, A.G., Daliakopoulos, I.N., Tsanis, I.K., 2017. A method to preserve trends in quantile mapping bias correction of climate modeled temperature. Earth Syst. Dyn. 8 https://doi.org/10.5194/esd-8-889-2017.
Grillakis, M.G., Koutroulis, A.G., Tsanis, I.K., 2013. Multisegment statistical bias correction of daily GCM precipitation output. J. Geophys. Res. Atmos. 118, 3150–3162. https://doi.org/10.1002/jgrd.50323.
Grillakis, M.G., Polykretis, C., Alexakis, D.D., 2020. Past and projected climate change impacts on rainfall erosivity: advancing our knowledge for the eastern Mediterranean island of Crete. CATENA 193, 104625. https://doi.org/10.1016/j.catena.2020.104625.
Haerter, J.O., Hagemann, S., Moseley, C., Piani, C., 2011. Climate model bias correction and the role of timescales. Hydrol. Earth Syst. Sci. 15, 1065–1079. https://doi.org/10.5194/hess-15-1065-2011.
Hasanpour Kashani, M., Dinpashoh, Y., 2012. Evaluation of efficiency of different estimation methods for missing climatological data. Stoch. Environ. Res. Risk Assess. 26, 59–71. https://doi.org/10.1007/s00477-011-0536-y.
Hennemuth, B., Bender, S., Bülow, K., Dreier, N., Keup-Thiel, E., Krüger, O., Mudersbach, C., Radermacher, C., Schoetter, R., 2013. Statistical Methods For the Analysis of Simulated and Observed Climate Data: Applied in Projects and Institutions Dealing With Climate Change Impact and Adaptation. CSC.
Jacob, D., Kotova, L., Teichmann, C., Sobolowski, S.P., Vautard, R., Donnelly, C., Koutroulis, A.G., Grillakis, M.G., Tsanis, I.K., Damm, A., Sakalli, A., van Vliet, M.T. H., 2018. Climate impacts in Europe under +1.5°C global warming. Earth's Future 6, 264–285. https://doi.org/10.1002/2017EF000710.
Jacob, D., Petersen, J., Eggert, B., Alias, A., Christensen, O.B., Bouwer, L.M., Braun, A., Colette, A., Déqué, M., Georgievski, G., Georgopoulou, E., Gobiet, A., Menut, L., Nikulin, G., Haensler, A., Hempelmann, N., Jones, C., Keuler, K., Kovats, S., Kröner, N., Kotlarski, S., Kriegsmann, A., Martin, E., van Meijgaard, E., Moseley, C., Pfeifer, S., Preuschmann, S., Radermacher, C., Radtke, K., Rechid, D., Rounsevell, M., Samuelsson, P., Somot, S., Soussana, J.F., Teichmann, C., Valentini, R., Vautard, R., Weber, B., Yiou, P., 2013. EURO-CORDEX: new high-resolution climate change projections for European impact research. Reg. Environ. Change 14, 563–578. https://doi.org/10.1007/s10113-013-0499-2.
Jones, G.V., White, M.A., Cooper, O.R., Storchmann, K., 2005. Climate change and global wine quality. Clim. Change 73, 319–343. https://doi.org/10.1007/s10584-005-4704-2.
Kottek, M., Grieser, J., Beck, C., Rudolf, B., Rubel, F., 2006. World map of the Köppen-geiger climate classification updated. Meteorol. Z. 15, 259–263. https://doi.org/10.1127/0941-2948/2006/0130.
Koufos, G., Mavromatis, T., Koundouras, S., Fyllas, N.M., Jones, G.V., 2014. Viticulture-climate relationships in Greece: the impacts of recent climate trends on harvest date variation. Int. J. Climatol. 34, 1445–1459. https://doi.org/10.1002/joc.3775.
Koufos, G.C., Mavromatis, T., Koundouras, S., Jones, G.V., 2018. Response of viticulture-related climatic indices and zoning to historical and future climate conditions in Greece. Int. J. Climatol. 38, 2097–2111. https://doi.org/10.1002/joc.5320.
Kuglitsch, F.G., Toreti, A., Xoplaki, E., Della-Marta, P.M., Zerefos, C.S., Trke, M., Luterbacher, J., 2010. Heat wave changes in the eastern mediterranean since 1960. Geophys. Res. Lett. 37 https://doi.org/10.1029/2009GL041841.
Lagarias, J.C., Reeds, J.A., Wright, M.H., Wright, P.E., 1998. Convergence properties of the nelder-mead simplex method in low dimensions. SIAM J. Optim. 9, 112–147. https://doi.org/10.1137/S1052623496303470.
Lazoglou, G., Anagnostopoulou, C., Koundouras, S., 2018. Climate change projections for Greek viticulture as simulated by a regional climate model. Theor. Appl. Climatol. 133, 551–567. https://doi.org/10.1007/s00704-017-2198-2.
Lorenz, D.H., Eichhorn, K.W., Bleiholder, H., Klose, R.B., Meier, U., Weber, E., 1994. Phänologische entwicklungsstadien der weinrebe (Vitis vinifera L. ssp. vinifera). Codierung Und Beschreibung nach Der Erweiterten BBCH-Skala.
Malheiro, A.C., Campos, R., Fraga, H., Eiras-Dias, J., Silvestre, J., Santos, J.A., 2013. Winegrape phenology and temperature relationships in the Lisbon wine region, Portugal. OENO One 47, 287. https://doi.org/10.20870/oeno-one.2013.47.4.1558.
Maraun, D., Wetterhall, F., Ireson, A.M., Chandler, R.E., Kendon, E.J., Widmann, M., Brienen, S., Rust, H.W., Sauter, T., Themeßl, M., Venema, V.K.C., Chun, K.P., Goodess, C.M., Jones, R.G., Onof, C., Vrac, M., Thiele-Eich, I., 2010. Precipitation downscaling under climate change: recent developments to bridge the gap between dynamical models and the end user. Rev. Geophys. 48, RG3003. https://doi.org/10.1029/2009RG000314.
Mascaro, G., Viola, F., Deidda, R., 2018. Evaluation of precipitation from EURO-CORDEX regional climate simulations in a small-scale mediterranean site. J. Geophys. Res. Atmos. 123, 1604–1625. https://doi.org/10.1002/2017JD027463.
Molina, M.O., Sánchez, E., Gutiérrez, C., 2020. Future heat waves over the Mediterranean from an Euro-CORDEX regional climate model ensemble. Sci. Rep. 10, 1–10. https://doi.org/10.1038/s41598-020-65663-0.
Molitor, D., Junk, J., Evers, D., Hoffmann, L., Beyer, M., 2014. A high-resolution cumulative degree day-based model to simulate phenological development of grapevine. Am. J. Enol. Vitic. 65, 72–80. https://doi.org/10.5344/ajev.2013.13066.
Mori, K., Goto-Yamamoto, N., Kitayama, M., Hashizume, K., 2007. Loss of anthocyanins in red-wine grape under high temperature. J. Exp. Bot. 58, 1935–1945. https://doi.org/10.1093/jxb/erm055.
Moss, R.H., Edmonds, J.A., Hibbard, K.A., Manning, M.R., Rose, S.K., van Vuuren, D.P., Carter, T.R., Emori, S., Kainuma, M., Kram, T., Meehl, G.A., Mitchell, J.F.B., Nakicenovic, N., Riahi, K., Smith, S.J., Stouffer, R.J., Thomson, A.M., Weyant, J.P., Wilbanks, T.J., 2010. The next generation of scenarios for climate change research and assessment. Nature 463, 747–756. https://doi.org/10.1038/nature08823.
Nerantzaki, S.D., Efstathiou, D., Giannakis, G.V., Kritsotakis, M., Grillakis, M.G., Koutroulis, A.G., Tsanis, I.K., Nikolaidis, N.P., 2019. Climate change impact on the hydrological budget of a large Mediterranean island. Hydrol. Sci. J. https://doi.org/10.1080/02626667.2019.1630741, 02626667.2019.1630741.
Nikulin, G., Bosshard, T., Yang, W., Bärring, L., Wilcke, R., Vrac, M., Vautard, R., Noel, T., Gutiérrez, J.M., Herrera, S., et al., 2015. Bias correction intercomparison project (BCIP): an introduction and the first results. In: Proceedings of the EGU General Assembly Conference Abstracts, p. 2250.
O'Neill, B.C., Kriegler, E., Riahi, K., Ebi, K.L., Hallegatte, S., Carter, T.R., Mathur, R., van Vuuren, D.P., 2014. A new scenario framework for climate change research: the concept of shared socioeconomic pathways. Clim. Change 122, 387–400. https://doi.org/10.1007/s10584-013-0905-2.
OIV, 2017. Distribution of the world's grapevine varieties. Int. Organ. Vine Wine 54.
Omazić, B., Telišman Prtenjak, M., Prša, I., Belušić Vozila, A., Vučetić, V., Karoglan, M., Karoglan Kontić, J., Prša, Ž., Anić, M., Šimon, S., Güttler, I., 2020. Climate change impacts on viticulture in Croatia: viticultural zoning and future potential. Int. J. Climatol. 40, 5634–5655. https://doi.org/10.1002/joc.6541.
Parker, A., de Cortázar-Atauri, I.G., Chuine, I., Barbeau, G., Bois, B., Boursiquot, J.M., Cahurel, J.Y., Claverie, M., Dufourcq, T., Gény, L., Guimberteau, G., Hofmann, R.W., Jacquet, O., Lacombe, T., Monamy, C., Ojeda, H., Panigai, L., Payan, J.C., Lovelle, B. R., Rouchaud, E., Schneider, C., Spring, J.L., Storchi, P., Tomasi, D., Trambouze, W., Trought, M., van Leeuwen, C., 2013. Classification of varieties for their timing of flowering and veraison using a modelling approach: a case study for the grapevine species Vitis vinifera L. Agric. For. Meteorol. 180, 249–264. https://doi.org/10.1016/j.agrformet.2013.06.005.

Parker, A.K., De Cortázar-Atauri, I.G., Van Leeuwen, C., Chuine, I., 2011. General phenological model to characterise the timing of flowering and veraison of Vitis vinifera L. Aust. J. Grape Wine Res. 17, 206–216. https://doi.org/10.1111/j.1755-0238.2011.00140.x.

Ramos, M.C., Jones, G.V., 2018. Relationships between Cabernet Sauvignon phenology and climate in two Spanish viticultural regions: observations and predicted future changes. J. Agric. Sci. 156, 1079–1089. https://doi.org/10.1017/S0021859618001119.

Riahi, K., Rao, S., Krey, V., Cho, C., Chirkov, V., Fischer, G., Kindermann, G., Nakicenovic, N., Rafaj, P., 2011. RCP 8.5-a scenario of comparatively high greenhouse gas emissions. Clim. Change 109, 33–57. https://doi.org/10.1007/s10584-011-0149-y.

Rosenzweig, C., Elliott, J., Deryng, D., Ruane, A.C., Müller, C., Arneth, A., Boote, K.J., Folberth, C., Glotter, M., Khabarov, N., Neumann, K., Piontek, F., Pugh, T.A.M., Schmid, E., Stehfest, E., Yang, H., Jones, J.W., 2014. Assessing agricultural risks of climate change in the 21st century in a global gridded crop model intercomparison. Proc. Natl. Acad. Sci. U. S. A. 111, 3268–3273. https://doi.org/10.1073/pnas.1222463110.

Ruml, M., Korać, N., Vujadinović, M., Vuković, A., Ivanišević, D., 2016. Response of grapevine phenology to recent temperature change and variability in the wine-producing area of Sremski Karlovci, Serbia. J. Agric. Sci. 154, 186–206. https://doi.org/10.1017/S0021859615000453.

Santibáñez, F., Sierra, H.F.G., Santibáñez, P.C., 2014. Degree day model of table grape (Vitis Vinifera l.) phenology in Mediterranean temperate climates. Int. J. Sci. Environ. Technol. 10–22. ISSN 2278-3687 3.

Scranton, K., Amarasekare, P., 2017. Predicting phenological shifts in a changing climate. Proc. Natl. Acad. Sci. U. S. A. 114, 13212–13217. https://doi.org/10.1073/pnas.1711221114.

Shabalala, Z.P., Moeletsi, M.E., Tongwane, M.I., Mazibuko, S.M., 2019. Evaluation of infilling methods for time series of daily temperature data: case study of Limpopo province, South Africa. Climate 7, 86. https://doi.org/10.3390/cli7070086.

Teslić, N., Vujadinović, M., Ruml, M., Ricci, A., Vuković, A., Parpinello, G.P., Versari, A., 2019. Future climatic suitability of the Emilia-Romagna (Italy) region for grape production. Reg. Environ. Change 19, 599–614. https://doi.org/10.1007/s10113-018-1431-6.

Themeßl, M.J., Gobiet, A., Heinrich, G., 2012. Empirical-statistical downscaling and error correction of regional climate models and its impact on the climate change signal. Clim. Change 112, 449–468. https://doi.org/10.1007/s10584-011-0224-4.

Thiébault, S., Moatti, J.P., Ducrocq, V., Gaume, E., Dulac, F., Hamonou, E., Shin, Y.J., Guiot, J., Cramer, W., Boulet, G., 2016. The Mediterranean region under climate change. A Sci. Updat. Marseille, IRD Éditions.

Tomasi, D., Jones, G.V., Giust, M., Lovat, L., Gaiotti, F., 2011. Grapevine phenology and climate change: relationships and trends in the Veneto region of Italy for 1964–2009. Am. J. Enol. Vitic. 62, 329–339. https://doi.org/10.5344/ajev.2011.10108.

Tonietto, J., Carbonneau, A., 2004. A multicriteria climatic classification system for grape-growing regions worldwide. Agric. For. Meteorol. 124, 81–97. https://doi.org/10.1016/j.agrformet.2003.06.001.

Tramblay, Y., Koutroulis, A., Samaniego, L., Vicente-Serrano, S.M., Volaire, F., Boone, A., Le Page, M., Llasat, M.C., Albergel, C., Burak, S., Cailleret, M., Kalin, K.C., Davi, H., Dupuy, J.L., Greve, P., Grillakis, M., Hanich, L., Jarlan, L., Martin-StPaul, N., Martínez-Vilalta, J., Mouillot, F., Pulido-Velazquez, D., Quintana-Seguí, P., Renard, D., Turco, M., Türkeş, M., Trigo, R., Vidal, J.P., Vilagrosa, A., Zribi, M., Polcher, J., 2020. Challenges for drought assessment in the Mediterranean region under future climate scenarios. Earth Sci. Rev. https://doi.org/10.1016/j.earscirev.2020.103348.

UNECE, 2017. United Nations economic commission for Europe—UNECE. UNECE standard FFV-19 concerning the marketing and commercial quality control of table grapes, 2017 Edition.

Urhausen, S., Brienen, S., Kapala, A., Simmer, C., 2011. Climatic conditions and their impact on viticulture in the Upper Moselle region. Clim. Change 109, 349–373. https://doi.org/10.1007/s10584-011-0059-z.

Verdugo-Vásquez, N., Fuente, C.P.D.L., Ortega-Farías, S., 2017. Model development to predict phenological scale of table grapes (cvs. Thompson, Crimson and Superior Seedless and Red Globe) using growing degree days. OENO One 51. https://doi.org/10.20870/OENO-ONE.2017.51.3.1833.

Wise, M., Calvin, K., Thomson, A., Clarke, L., Bond-Lamberty, B., Sands, R., Smith, S.J., Janetos, A., Edmonds, J., 2009. Implications of limiting CO_2 concentrations for land use and energy. Science 324, 1183–1186. https://doi.org/10.1126/science.1168475.

Zapata, D., Salazar, M., Chaves, B., Keller, M., Hoogenboom, G., 2015. Estimation of the base temperature and growth phase duration in terms of thermal time for four grapevine cultivars. Int. J. Biometeorol. 5912 (59), 1771–1781. https://doi.org/10.1007/S00484-015-0985-Y, 2015.

Zittis, G., Hadjinicolaou, P., Klangidou, M., Proestos, Y., Lelieveld, J., 2019. A multi-model, multi-scenario, and multi-domain analysis of regional climate projections for the Mediterranean. Reg. Environ. Change 19, 2621–2635. https://doi.org/10.1007/s10113-019-01565-w.